BMC Complementary Medicine and Therapies

RESEARCH

Open Access

Integrated transcriptomic and functional analysis reveals selective cytotoxicity and HPV oncogene suppression induced by cinnamon essential oil in cervical cancer cells

Ruben Piña-Cruz[1,2†], Andrea Molina-Pineda[3†], Sayma Vizcarra-Ramos[4], Jesús García-Gómez[4], Mariel García-Chagollán[5], Rodolfo Hernández-Gutiérrez[3], Luis Felipe Jave-Suarez[2*] and Adriana Aguilar-Lemarroy[6*]

Abstract

Background Cervical cancer (CC) remains a major cause of cancer-related mortality among women worldwide, primarily driven by persistent infection with high-risk human papillomavirus (HPV) types. Given that natural products with selective antitumour properties offer potential for novel therapies, we evaluated the cytotoxic, antiproliferative, and molecular effects of *cinnamon* essential oil (CEO) on HPV-positive cervical cancer cell lines (HeLa and SiHa) and nontumorigenic keratinocytes (HaCaT).

Methods Cells were exposed to a range of dilutions of CEO. Cell viability was determined by WST-1 and sulforhodamine B assays. Apoptosis was assessed using Annexin V/PI staining, caspase-3/8/9 activation, and mitochondrial membrane potential (Δψm) loss by flow cytometry. Proliferation was measured using EdU incorporation, and senescence was measured by β-galactosidase activity. Genome-wide transcriptional changes and HPV E6/E7 oncogene expression were analysed by RNA-Seq and validated with qPCR.

Results CEO induced dose-dependent cytotoxicity and inhibited proliferation in cervical cancer cells, while HaCaT cells were significantly more resistant. Apoptosis was evidenced by Annexin V/PI positivity, activation of caspases -8, -9, and -3, and significant loss of mitochondrial membrane potential. No significant senescence induction was observed. Additionally, CEO also significantly downregulated HPV *E6/E7* oncogene expression in HeLa and SiHa cells. Transcriptomic analysis revealed broad differential gene expression, including upregulation of stress and apoptosis-related genes and downregulation of proliferation, oxidative phosphorylation, and viral-related pathways.

†Ruben Piña-Cruz and Andrea Molina-Pineda contributed equally to this work.

*Correspondence:
Luis Felipe Jave-Suarez
luis.jave@academicos.udg.mx
Adriana Aguilar-Lemarroy
adriana.aguilar@academicos.udg.mx

Full list of author information is available at the end of the article

© The Author(s) 2026. **Open Access** This article is licensed under a Creative Commons Attribution 4.0 International License, which permits use, sharing, adaptation, distribution and reproduction in any medium or format, as long as you give appropriate credit to the original author(s) and the source, provide a link to the Creative Commons licence, and indicate if changes were made. The images or other third party material in this article are included in the article's Creative Commons licence, unless indicated otherwise in a credit line to the material. If material is not included in the article's Creative Commons licence and your intended use is not permitted by statutory regulation or exceeds the permitted use, you will need to obtain permission directly from the copyright holder. To view a copy of this licence, visit http://creativecommons.org/licenses/by/4.0/.

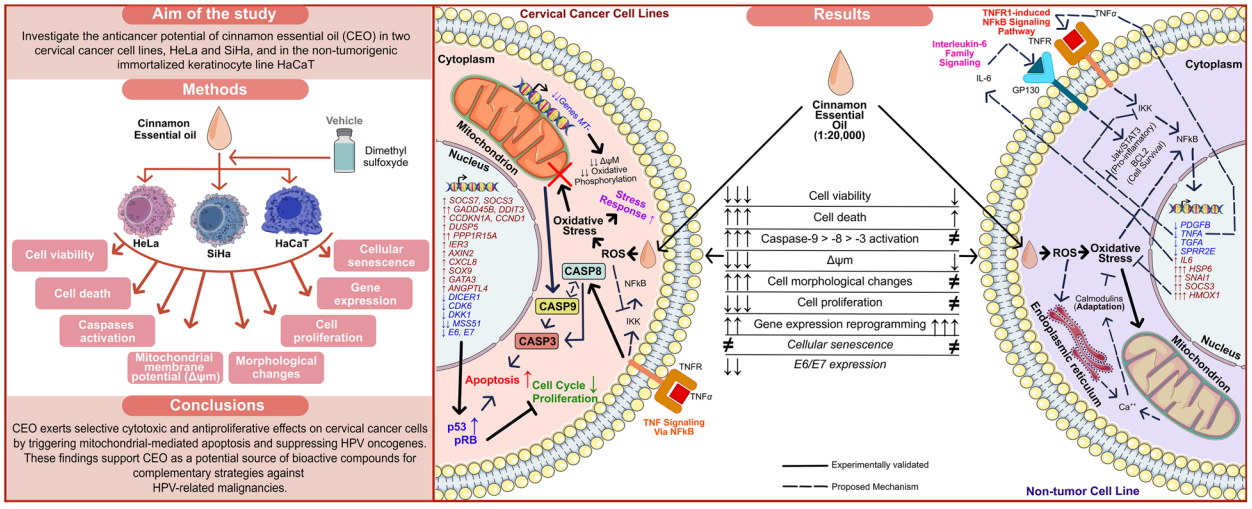
Conclusion CEO exerts selective cytotoxic and antiproliferative effects on cervical cancer cells by triggering mitochondria-mediated apoptosis and suppressing HPV oncogenes. These findings support CEO as a potential source of bioactive compounds for complementary strategies against HPV-related malignancies.

Highlights

- CEO shows dose-dependent and selective killing of cervical cancer cells.
- CEO reduces proliferation without inducing senescence.
- CEO triggers apoptosis via mitochondrial depolarization and caspase activation.
- HPV E6 and E7 oncogenes are downregulated by CEO in tumor cells.
- CEO modulates p53, TNFα/NF-κB, and mTORC1 pathways in cancer lines.

Keywords *Cinnamon* essential oil, *Cinnamomum zeylanicum*, Cervical cancer, Apoptosis, Mitochondrial pathway, HPV E6/E7

Graphical Abstract



Background

Cervical cancer remains a major public health issue, with an estimated 662,301 new cases and 348,874 deaths worldwide in 2022. It is the fourth most common malignancy and cause of cancer death among women globally, following breast, colorectal, and lung cancers [1–3]. Although the disease is largely preventable, nearly 90% of deaths occur in low- and middle-income countries, reflecting stark global inequalities [4]. Persistent infection with high-risk human papillomavirus (HPV) types, particularly HPV-16 and HPV-18, is the principal etiological factor driving cervical carcinogenesis [5–9]. The viral oncoproteins E6 and E7 play pivotal roles in this process by inactivating the key tumor suppressors p53 and pRb, thereby promoting uncontrolled cell proliferation, evasion of apoptosis, and genomic instability [10–14]. Despite advances in screening, vaccination, and therapeutic strategies, treatment options for established cervical cancer remain limited. Furthermore, current chemotherapeutic regimens often result in cytotoxic side effects and the emergence of drug resistance [15–17]. Therefore, there is an urgent need to identify novel, effective, and safer therapeutic alternatives.

In recent years, the World Health Organization (WHO) has emphasized the importance of exploring bioactive compounds derived from natural or plant-based sources as part of its global strategy to develop innovative, accessible, and sustainable therapeutic agents [18]. Natural products have historically been a cornerstone in drug discovery, providing structurally diverse molecules with potent biological activities [19–21]. In this context, essential oils and their active constituents have attracted attention due to their multifaceted pharmacological effects, including antioxidant, anti-inflammatory, antimicrobial, and anticancer properties [22–27]. Investigating their molecular mechanisms of action may contribute to the discovery of new agents that complement or enhance conventional cancer therapies.

Among these, cinnamon essential oil (CEO), extracted from *Cinnamomum zeylanicum*, has demonstrated a broad spectrum of biological activities, including antioxidant, antimicrobial, and antitumour effects in various

cancer models [28–32]. Its main bioactive component, cinnamaldehyde, has been reported to modulate key cellular processes such as oxidative stress, apoptosis, and mitochondrial function [33–41]. Despite growing evidence of CEO's biological activity, comprehensive insights into its molecular mechanisms in cervical cancer are still limited. Notably, there are no comprehensive transcriptomic studies addressing how CEO modulates gene expression, signalling pathways, or viral oncogene activity in cervical cancer models.

In this study, we aimed to investigate the anticancer potential of CEO in two cervical cancer cell lines, HeLa and SiHa, and in the nontumorigenic immortalized keratinocyte line HaCaT. We evaluated CEO's ability to reduce cell viability, induce apoptosis, and elicit characteristic morphological changes associated with programmed cell death. In addition, caspase activation, mitochondrial membrane potential alterations, proliferation, and cellular senescence were assessed to delineate its cytotoxic mechanisms. To further explore its molecular impact, we conducted next-generation RNA sequencing (RNA-seq) followed by transcriptomic and pathway enrichment analyses, alongside quantitative PCR (qPCR) validation of key genes and protein–protein interaction analyses. Importantly, we also examined CEO's effect on the expression of HPV *E6* and *E7* oncogenes. Together, these findings will provide new insights into the cellular and molecular responses elicited by CEO and support its potential as a promising natural compound with therapeutic relevance in cervical cancer.

Methods

Cells and cell culture

All cervical cancer cell lines, as well as the nontumorigenic human epithelial cell line HaCaT, were obtained from the German Cancer Research Center (DKFZ, Heidelberg, Germany) and authenticated using multiplex human cell line authentication tests conducted by Multiplexion GmbH (Friedrichshafen, Germany). Cells were cryopreserved in liquid nitrogen until they were required for experiments. For use, cells were quickly thawed in a 37 °C water bath and centrifuged at 1,000 rpm for 10 min to remove residual dimethyl sulfoxide from the freezing process. The resulting cell pellet was then resuspended in fresh Dulbecco's modified Eagle's medium (DMEM) supplemented with L-glutamine (584 mg/L), sodium pyruvate (110 mg/L), D-glucose (1 g/L) (Cat. No. 10567–014 Gibco, Thermo Fisher Scientific, Waltham, MA, USA), 10% fetal bovine serum (FBS) (Cat. No. 35–010-CV, Corning, NY, USA), penicillin (100 U/mL), streptomycin (100 µg/mL) and amphotericin (0.25 µg/mL) (Cat. No. 15240–062 Gibco, Thermo Fisher Scientific, Waltham, MA, USA). Cell cultures were maintained at 37 °C in a humidified atmosphere with 5% CO_2 and grown until reaching 80–90% confluence. Once confluence was achieved, the cells were detached with 0.25% trypsin–EDTA (Cat. No. 25–053-CI Corning, Manassas, VA, USA) for subsequent experiments.

Reagents

The cinnamon essential oil (CEO), Cinnamon® (*Cinnamomum zeylanicum*, Lot No. 30030608), was obtained from dōTERRA® International (Pleasant Grove, UT, USA). According to the manufacturer's certificate of analysis, the major bioactive constituents include cinnamaldehyde (50–70%), cinnamyl acetate (2–15%), and eugenol (1–10%). The essential oil was diluted at a 1:2 ratio in dimethyl sulfoxide (DMSO; Cat No. 67–68-5 Sigma–Aldrich, MA, USA) to prepare a stock solution (CEO-DMSO).

Treatments preparation

Treatment dilutions were prepared to the following final concentrations by diluting the CEO-DMSO stock solution in fresh supplemented DMEM: 1:40,000 (26.75 µg/mL), 1:20,000 (53.5 µg/mL), 1:15,000 (71.33 µg/mL), 1:12,500 (85.6 µg/mL), 1:10,000 (107.0 µg/mL), 1:5,000 (214.0 µg/mL), 1:1,000 (1,070.0 µg/mL), and 1:500 (2,140.0 µg/mL). These concentrations were calculated based on the density of the essential oil (approximately 1.07 mg/µL).

Cell viability assay

Cells were seeded in 96-well, flat-bottom, tissue-culture-grade microplates (Cat: 83.3924 Sarstedt, Nümbrecht, Germany) at densities of 2.5×10^4 for HeLa, 3×10^4 for SiHa, and 4×10^4 for HaCaT cells per well. The plates were incubated at 37 °C in a humidified atmosphere with 5% CO_2. Treatment dilutions were prepared at the following concentrations: 1:40,000, 1:20,000, 1:15,000, 1:12,500, 1:10,000, 1:5,000, 1:1,000, and 1:500 using the CEO-DMSO stock solution in fresh supplemented DMEM (as described in the cell culture section). A 1:500 dilution of DMSO in supplemented DMEM was used as the vehicle control. Treatments were performed in sextuplicate at 100 µL per well, including untreated and vehicle-only controls. The plates were incubated for 24 h at 37 °C in 5% CO_2. After treatment, 10 µL of WST-1 cell proliferation reagent (Cat. No. 05–015–944–001, Roche Diagnostics, Mannheim, Germany) was added to each well. Absorbance was measured at 480 nm with correction at 600 nm after 2 and 3 h using a Sinergy HT multimode microplate reader (Cat. No. 7091000, BioTek Instruments, Inc., Winooski, VT). The 50% inhibitory concentration (IC_{50}) was calculated using the formula previously used by Piña-Cruz et al. [42], which was originally described by Sebaugh.

Cell death determination

Cells were seeded in 12-well plates (Cat. No. 83.3921 Sarstedt, Nümbrecht, Germany) at densities of 2.5×10^5 for HeLa cells, 3×10^5 for SiHa cells, and 4×10^5 for HaCaT cells per well and incubated overnight in supplemented DMEM. The cells were then treated with CEO at dilutions of 1:40,000, 1:20,000, 1:15,000, 1:12,500, 1:10,000, 1:5,000, 1:1,000, or 1:1,000 DMSO solution as a vehicle control for 24 h. After treatment, the cells were detached with trypsin and stained using the FITC Annexin V Apoptosis Detection Kit with propidium iodide (PI) protocol (Cat. No. 640914, BioLegend, CA, USA) according to the manufacturer's instructions. Samples were analysed by flow cytometry (Beckman Coulter Cytoflex), acquiring a minimum of 10,000 events per sample. Cells positive for PI, annexin V (AV), or both (PI^+/AV^+) were considered dead, while double-negative (PI^-/AV^-) cells were considered viable.

Visualization of microscopic cellular damage

Cells were seeded in 12-well plates (Sarstedt, Cat: 83.3921, Nümbrecht, Germany) at a density of 2.5×10^5 for HeLa, 3×10^5 for SiHa, and 4×10^5 for HaCaT per well. CEO dilutions of 1:20,000, 1:15,000, 1:12,500, 1:10,000, and 1:5,000 were prepared in supplemented DMEM, along with a 1:5,000 DMSO vehicle control. After 24 h of incubation, photomicrographs were acquired using a ZEISS Primovert inverted cell culture microscope equipped with an AxioCam ERc 5 s camera using a 40 × objective (Carl Zeiss, Germany). Images were captured and processed using ZEISS ZEN software (v. 3.8.1).

Cell proliferation (EdU incorporation assay)

Cells were seeded in 12-well plates at densities of 2×10^5 (HeLa), 2.5×10^5 (SiHa), and 4×10^5 (HaCaT) cells per well. Following overnight incubation, the cells were treated for 24 h with DMSO, CEO (1:20,000), or doxorubicin (1 μM). This time point, selected based on preliminary time-course experiments and IC_{50} values from the WST-1 assay, corresponds to a stage at which CEO-induced cytotoxicity was already apparent, allowing for the capture of early antiproliferative responses before extensive cell death occurred and thus enabling a clearer assessment of DNA synthesis inhibition. A uniform 24-h exposure was applied across all cell lines to allow direct comparisons, regardless of differences in their doubling times. After treatment, the cells were incubated with 10 mM EdU for 4 h at 37 °C and 5% CO_2 and then fixed and permeabilized using the EdU Cell Proliferation Kit with iFluor 647 Azide (Cat. No. ab222421 Abcam Cambridge, MA, USA). Fluorescence was analysed by a Cytek Aurora spectral flow cytometer (Cytek Biosciences, Fremont, CA, USA). Data acquisition was performed using SpectroFlo™ software (v.3.0.1), and analysis was conducted with FlowJo™ software (v.10.9.0, BD Biosciences Ashland, OR, USA). This cytometer and software were used in the subsequent flow cytometry assays.

Cell viability (Sulforhodamine B Assay)

Cells were plated in 96-well plates at the following densities: 5×10^3 for HeLa, 6.25×10^3 for SiHa, and 1×10^4 for HaCaT. After 24 h of incubation, cells were treated with CEO dilutions (1:40,000, 1:30,000, 1:20,000, and 1:10,000), DMSO (vehicle control), and doxorubicin (0.5 μM and 1 μM) as a positive control for 72 h. Without removing the medium, 50 μL of fixative was added to each well, and the plates were incubated at 4 °C for 1 h. The wells were then washed three times with distilled water, stained with 45 μL of sulforhodamine B (Cat. No. ab235935 Abcam Cambridge, MA, USA) for 15 min, washed four times, and air-dried. Microscopy images were captured with a ZEISS Primovert inverted cell culture microscope using a 40 × objective. Bound dye was solubilized in 200 μL of 10 mM Tris base (pH 10.5), which is the standard buffer recommended for this step. The plates were gently shaken for 10 min at room temperature, and the absorbance was measured at 565 nm using a Synergy HT microplate reader.

Caspase-3, −8, and −9 activation

HeLa, SiHa, and HaCaT cells were seeded in 12-well plates at densities of 2×10^5, 2.5×10^5, and 3×10^5 cells per mL, respectively, in 1 mL of supplemented DMEM. After 24 h, the cells were treated with CEO (1:20,000 dilution) for an additional 24 h at 37 °C with 5% CO_2. Following treatment, cells were harvested, washed once with PBS, detached with trypsin–EDTA and stained with caspase 3, 8 or 9 activity assay kits (Abcam, Cat. Nos. ab65613, ab65614, ab65615, respectively), according to the manufacturer's protocols. Stained samples were analysed by spectral flow cytometry. Mean fluorescence intensity (MFI) values were obtained using FlowJo software (v.10.9.0, BD Biosciences Ashland, OR, USA) and plotted in GraphPad Prism (v.8.0.2, San Diego, CA, USA).

Mitochondrial membrane potential

HeLa (2×10^5), SiHa (2.5×10^5), and HaCaT (4×10^5) cells were seeded in 12-well plates with 1 mL of DMEM and incubated overnight. Afterwards, the cells were treated with DMSO or CEO (1:20,000) for 24 h. After treatment, the cells were harvested, washed once with PBS, detached with trypsin–EDTA, transferred to labelled flow cytometry tubes, and centrifuged at 1,000 rpm for 10 min. The resulting cell pellets were resuspended in 500 μL of staining solution (prepared by diluting 1 μL of JC-10 dye in 5 mL of assay buffer (Cat. No. ab112133 Abcam, Cambridge, MA, USA)) and incubated for 30 min at 37 °C with 5% CO_2. Samples were analysed immediately by

spectral flow cytometry. The red/green fluorescence ratio (570/520 nm) was calculated based on the MFI values and plotted using GraphPad Prism (v.8.0.2, GraphPad Software, San Diego, CA, USA).

Induction and assessment of cellular senescence

Cells were seeded in 12-well plates at 1×10^5 (HeLa), 1.2×10^5 (SiHa), and 1.6×10^5 (HaCaT) cells per well in 1 mL of medium. After overnight incubation, the cells were treated with DMSO, CEO (1:20,000), or doxorubicin (2 µM) for 48 h. Senescence was assessed using the Senescence Detection Kit for Flow Cytometry (Cat. No. ab228562 Abcam, Cambridge, MA, USA). Following treatment, the cells were stained for 1 h at 37 °C according to the manufacturer´s instructions, washed twice, and resuspended in 300 µL of assay buffer for immediate analysis by spectral flow cytometry. Data were analysed using FlowJo™ software (v.10.9.0, BD Biosciences, Ashland, OR, USA).

RNA extraction

Cells were seeded in 100 mm tissue culture dishes (Cat. No. 430167 Corning, NY, USA) at densities of 2.5×10^6 for HeLa, 3×10^6 for SiHa, and 4×10^6 for HaCaT cells. After overnight incubation, the cells were treated with a 1:20,000 dilution of CEO or DMSO (vehicle control) for 4 h. Total RNA was isolated using the Quick-RNA Mini-Prep kit (Cat. No. R1055, Zymo Research Corp., Irvine, CA, USA) following the manufacturer's instructions. The RNA concentration was determined by measuring absorbance at 260/280 nm using the Synergy HT microplate reader and stored at −80 °C until use.

RNA-Seq analysis

RNA integrity was assessed with a Bioanalyzer 2100 (Agilent Technologies, Santa Clara, CA, USA) using the Agilent RNA 6000 Nano Kit (Cat. No. 6067–1511 Agilent Technologies, Santa Clara, CA, USA). Only samples with RNA integrity numbers (RIN) > 7 were used for sequencing. A total of 3.0 µg of RNA per sample was submitted to Novogene Corporation Inc. (Sacramento, CA, USA) for next-generation sequencing using NovaSeq 6000 technology (Illumina, San Diego, CA, USA). The experiment included two biological replicates per condition (CEO-treated and DMSO vehicle control) for each cell line (HeLa, SiHa, and HaCaT). The raw sequencing data have been deposited in the GEO Data repository under the accession number GSE311189.

Bioinformatics

Raw reads were analysed using R (v. 4.3.1), RStudio (v. 2023.09.1 + 494), and the Galaxy platform (https://www.usegalaxy.org, accessed August 2024). Quality was assessed with the FastQC tool (Galaxy, V. 0.74 + galaxy0). Reads were mapped and aligned to the Human Reference Genome GRCh38.p14v46 using the align function from the Rsubread package (Ver. 2.14.2). The resulting BAM files were used to generate read count tables with the FeatureCounts function. Differentially expressed genes (DEGs) were identified with DESeq2 (v. 1.42. 0) R package. The enrichment analysis was performed using the Kyoto Encyclopedia of Genes and Genomes (KEGG) database in R using the PathFindeR package (v. 2.3.1) and hallmark gene data sets using Gene Set Enrichment Analysis (GSEA) software (v. 4.3.2) [43].

Protein–Protein Interaction (PPI) network analysis

To explore interactions among proteins encoded by the differentially expressed genes (DEGs) identified through RNA-seq, only genes meeting the criteria of adjusted p value (*padj*) < 0.05 and $|\log_2$ fold change (FC)$| \geq 2.0$ were selected. These DEGs were uploaded to the STRING database (https://string-db.org/) using the "Multiple proteins" option with *Homo sapiens* set as the reference organism. A minimum interaction confidence score of 0.4 ~ 0.7 was applied. Unconnected proteins were filtered out to improve clarity and focus on biologically relevant interactions.

Quantitative Polymerase Chain Reaction (qPCR)

Total RNA, isolated as previously described, was used for quantitative polymerase chain reaction (qPCR). Complementary deoxyribonucleic acid (cDNA) synthesis was performed using the Transcriptor First Strand cDNA Synthesis Kit (Cat. No. 04 379 012 001, Roche Diagnostics, Basel, Switzerland). qPCR was carried out on the LightCycler 2.0 platform (Roche Diagnostics, Basel, Switzerland) using the LightCycler FastStart DNA Master plus SYBR Green I Kit (Cat. No. 03515869001, Roche Diagnostics, Basel, Switzerland). Primers were designed using the NCBI Primer-BLAST tool (https://www.ncbi.nlm.nih.gov/tools/primer-blast/). The expr ession data were normalized using *RPS18*, *RPLP0, and GAPDH* as reference genes. Primer sets for the target genes (*HSPA6*, *GADD45B*, *PPP1R15A*, *HMOX1*, *ATF3*, *DDIT3*, *CDKN1A*, *MT-CO1*, *MT-CO2*, *MTCO2P12*, *MT-CO3*, *CCND1*, *JUN*, *EGR1*, *PGF*, *KLHL24*, *SNAI1*, *SOCS3*, *PMAIP1*, *E6* HPV-16, *E6* HPV-18, *E7* HPV16, *E7* HPV18) are summarized in Table 1. The results were analysed using LightCycler Software v. 4.1, and relative gene expression was calculated using the $2^{-}\Delta\Delta$Cp method and expressed as $\log_2$ fold change.

Results

Cinnamon essential oil induces cell death and reduces viability in a dose-dependent manner in cervical cancer cell lines

To evaluate the cytotoxic effects of CEO on cervical cancer cell lines (HeLa and SiHa) and nontumorigenic

Table 1 Primer sequences and qPCR conditions for target gene expression analysis. The table includes the forward (F-) and reverse (R-) primer sequences, amplicon length, and annealing temperature for each target gene

Gene	Sequence (5′–3′)	Amplicon length (pb)	Annealing temp (°C)
ATF3	F-TCT GCG CTG GAA TCA GTC R-CTC CTT CTT CTT GTT TCG GCA C	150	59
CCND1	F-CGC ACG ATT TCA TTG AAC AC R-CAG CAG GGC TTC GAT CTG	296	60
CDKN1A	F-TGT ACC CTT GTG CCT CGC T R-GCT TCC TGT GGG CGG ATT A	163	64
DDIT3	F-TTC AGA TGA AAA TGG GGG TAC R-ACC ACT CTG TTT CCG TTT CC	238	62
E6 HPV-16	F-GAG ACA TTT TAT GCA CCA AA R-CTC CAT GCA TGA TTA CAG C	499	60
E6 HPV-18	F-AAT ACT ATG GCG CGC TTT GA R-TTG CCT TAG GTC CAT GCA TAC T	510	60
E7 HPV-16	F-TAG AGA AAC CCA GCT GTA ATC A R-AGG ATC AGC CAT GGT AGA TTA T	336	60
E7 HPV-18	F-CGC AGA GAA ACA CAA GTA TAA T R-GAT CAG CCA TTG TTG CTT A	363	60
EGR1	F- GAA CGC AAG CAT ACC A R- GGT TGC TGT CAT GTC CGA AAG	375	60
GADD45B	F-CAT CAA CAT CGT GCG GGT GT R-GTA GGG GAC CCA CTG GTT GT	205	66
GAPDH	F-CAC TGC CAC CCA GAA GAC TGT G R-TGT AGG CCA TGA GGT CCA CCA C	449	56
HMOX1	F-CTG CTG ACC CAT GAC ACC AA R-CAA CTG TCG CCA CCA GAA AG	187	61
HSPA6	F-CCA GAG GAA CGC CAC TAT CC R-GGA GGG ATG CCA CTG AGT TC	156	62
JUN	F- TGG AAA GTA CTC CCC TAA CCT R- CTG AAA CAT CGC ACT ATC CTT	250	58
KLHL24	F- GAA AGG GAA AGG AGA AGC AGG A R- GAG GAC AGC CAT TTT GTG ACG	263	62
MT-CO1	F-CGA CGT TAC TCG GAC TAC CC R-GAA TGT GTG GTA GGG TGG GG	204	62
MT-CO2	F-GTA CTC CCG ATT GAA GCC CC R-CGA TGG GCA TGA AAC TGT GG	202	62
MTCO2P12	F-GGT TGA AGC CCC CAT TCG TA R-TTC AGA GCA TTG GCC GTA GT	160	61
MT-CO3	F-CGG CAT CTA CGG CTC AAC AT R-AAT GCC AGT ATC AGG CGG C	161	61
PDF	F- AAG GGG GCC CTG CTA CCT GT R- CCC CAG GCA ACC ACT GTT CTC	218	62
PMAIP1	F-GAG ATG CCT GGG AAA AAG G R-TCC TGA GCA GAA GAG TTT GGA	313	58
PPP1R15A	F-TTC CGA GTG GCC ATC TAT GT R-ATG GAC AGT GAC CTT CTC GG	177	59
RPLP0	F-CCT CAT ATC CGG GGG AAT GTG R-GCA GCA GCT GGC ACC TTA TTG	95	58
RPS18	F-CGA TGG GCG GCG GAA AA R-CAG TCG CTC CAG GTC TTC ACG G	283	60
SNAI1	F- CGA AAG GCC TTC AAC TGC AA R- CGC CTG GCA CTG GTA CTT CTT	270	60
SOCS3	F- CAA GGA CGG AGA CTT CGA TTC R- GGT CAC TGC GCT CCA GTA GAA	273	60

keratinocytes (HaCaT), we assessed cell viability using the WST-1 assay and cytotoxicity by Annexin V/Propidium Iodide (AV/PI). Cells were treated with a range of dilutions of CEO from 1:40,000 to 1:500. DMSO was also included as vehicle-treated cells and showed no significant differences compared to untreated cells (Control).

As shown in Fig. 1a, CEO exhibited a dose-dependent effect on cell viability (WST-1 assay), with IC_{50} values of 1:40,000 for HeLa, 1:25,000 for SiHa, and 1:15,400 for HaCaT cells, indicating that HaCaT cells were the most resistant. The most pronounced difference occurred at the 1:20,000 dilution, and CEO reduced cell viability to 20.8% in HeLa, 33.2% in SiHa, and 83.2% in HaCaT ($p < 0.05$).

CEO-induced cytotoxicity was confirmed to be due to cell death, as shown by Annexin V/Propidium Iodide (AV/PI) staining (Fig. 1b), showing massive cell death (78.2%) in HeLa cells and 24.6% in SiHa cells at the same dilution versus only 15.6% in HaCaT cells. The IC_{50} values derived from the AV/PI assay were 1:66,670 for HeLa, 1:20,250 for SiHa, and 1:10,000 for HaCaT, reflecting the greater sensitivity of the apoptosis assay compared to the metabolic activity assay. Based on these results, a 1:20,000 dilution was selected for subsequent experiments.

Morphological changes and EdU incorporation assays validate the antiproliferative effect of cinnamon essential oil

To evaluate the effect of cinnamon essential oil (CEO) on cell morphology, CC-derived cell lines and nontumorigenic HaCaT keratinocytes were exposed to a 1:20,000 dilution for 24 h. As shown in Fig. 2a, phase-contrast microscopy revealed marked morphological alterations in CEO-CC-treated cells, including cell rounding, shrinkage, and detachment, consistent with apoptotic death. In contrast, DMSO-treated cells maintained a confluent monolayer with intact cell–cell junctions and typical

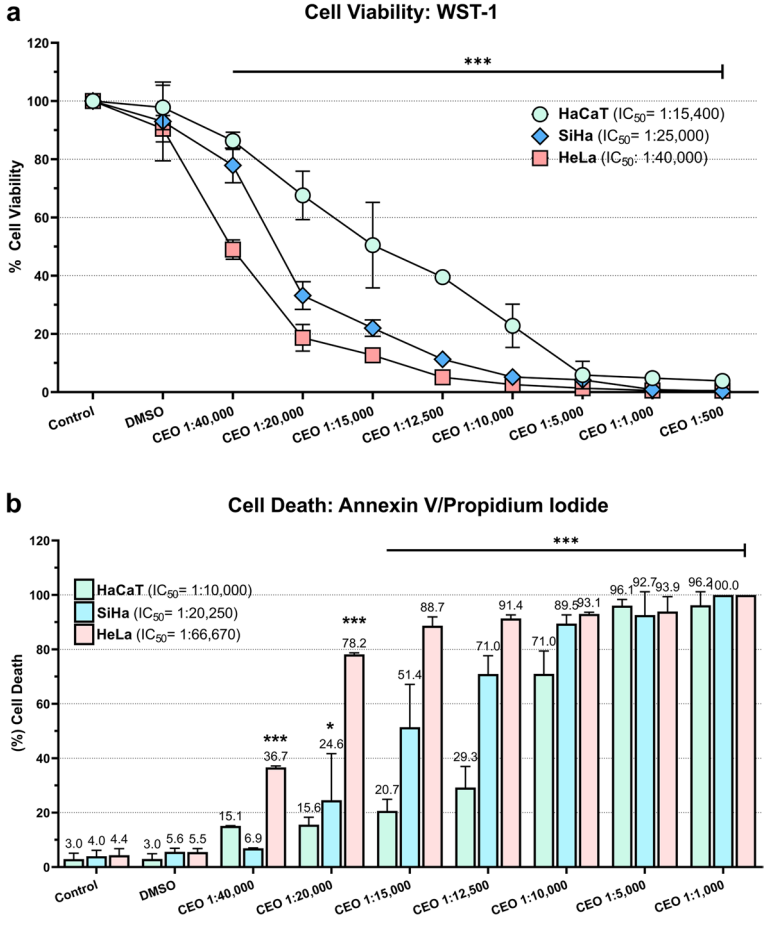


Fig. 1 Cytotoxic effect of cinnamon essential oil (CEO) on cervical cancer cells and nontumorigenic keratinocytes. **a** WST-1 viability assay showing the percentage of viable cells after 24 h of treatment with increasing CEO concentrations. Untreated cells (control) and cells treated only with vehicle (DMSO) were included. The half-maximal inhibitory concentration (IC_{50}) values are indicated for each cell line. In addition, cell death was quantified in parallel by (**b**) Annexin V/Propidium Iodide (PI) staining performed by cytometry. Annexin V–positive, PI–positive, and double-positive populations were collectively considered dead cells. Data are presented as the mean ± SD from three independent experiments. Statistical significance is indicated as ***$p < 0.001$ vs. control

epithelial morphology (consistent with untreated controls from preliminary experiments), and HaCaT cells exhibited no significant changes upon CEO treatment.

Based on these cytotoxic effects, we next examined whether CEO also affects cell proliferation using a 5-ethynyl-2′-deoxyuridine (EdU) incorporation assay. As illustrated in Fig. 2b, CEO treatment for 24 h significantly reduced cell proliferation in HeLa and SiHa cells ($p < 0.001$), demonstrating a strong antiproliferative effect. Interestingly, in nontumorigenic HaCaT cells, CEO did not inhibit proliferation and instead induced a slight, nonsignificant increase.

Cinnamon essential oil selectively and potently reduces cellular biomass in cervical cancer cells

To further corroborate the antiproliferative effect of CEO, cell viability was assessed using the sulforhodamine B (SRB) assay. Consistent with previous WST-1 and EdU results, microscopic examination revealed that CEO treatment (1:20,000) caused a marked loss of cell density,

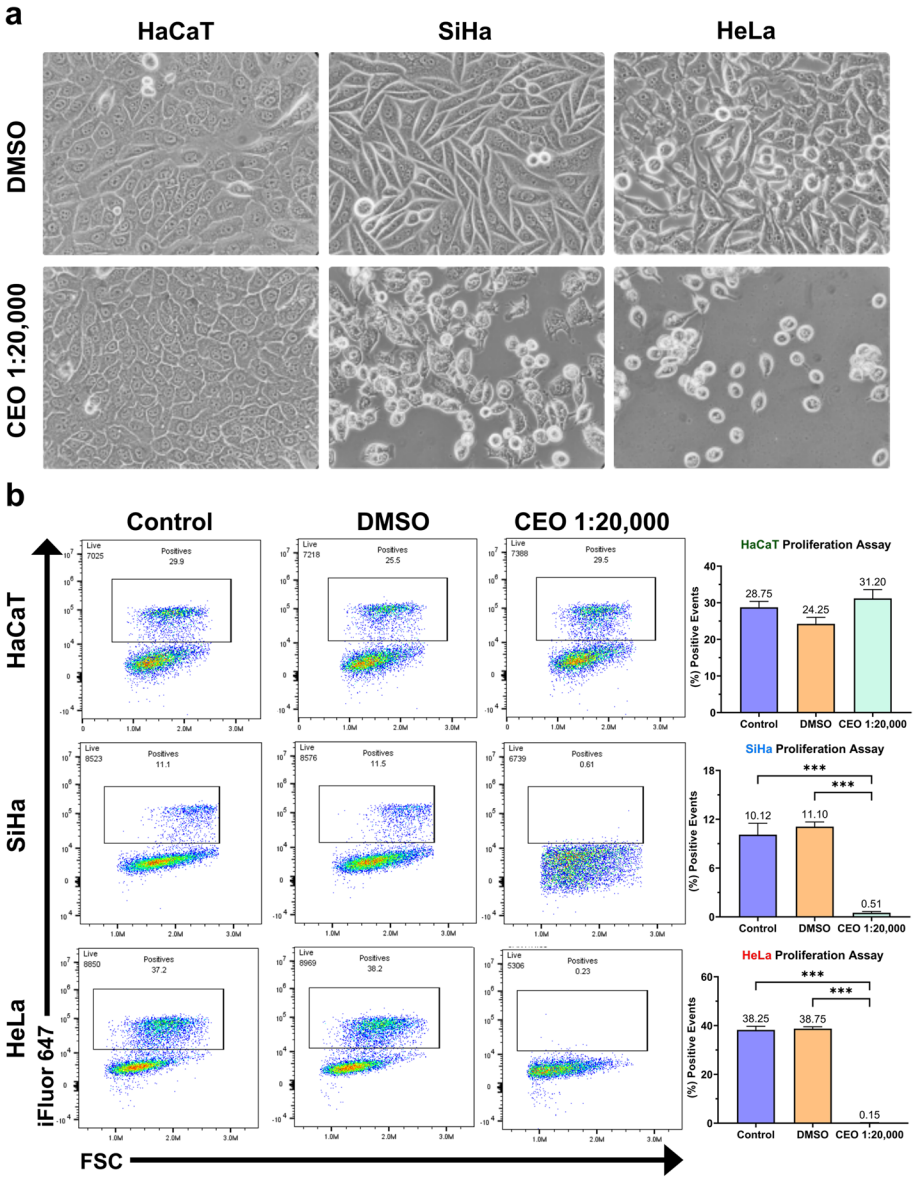


Fig. 2 Morphological changes and cell proliferation assay after 24 h of incubation with CEO. **a** Phase-contrast microscopy images (40× magnification) depict the morphological alterations in HaCaT, SiHa, and HeLa cells treated with DMSO or CEO (1:20,000 dilution). **b** Cell proliferation assay measured by EdU incorporation, detected with iFluor 647, and analysed by flow cytometry. Representative dot plots display forward scatter (FSC-A) versus EdU–iFluor 647 fluorescence intensity. The gated region indicates EdU-positive cells actively undergoing DNA synthesis. On the right side of the figure, bar graphs summarize the percentage of EdU-positive cells for each condition across the four cell lines. Statistical significance is indicated as ***$p < 0.001$ compared to the control group

diminished staining intensity, and morphological features of cytotoxicity, such as shrinkage and detachment (Fig. 3a). In contrast, HaCaT cells retained their morphology and staining intensity. DMSO-treated controls exhibited uniform SRB staining, high cell density, and intact morphology in all cell lines, indicating preserved viability.

Quantitative analysis of SRB absorbance confirmed these morphological observations (Fig. 3b). In HeLa cells, CEO reduced cell viability to below 14% in all tested dilutions (1:40,000 to 1:10,000). In SiHa cells, a clear dose-dependent decrease was observed (56.2% to 31.2% viability) ($p < 0.001$). Conversely, HaCaT viability remained above 96% except at the highest CEO concentration (1:10,000), where it was 81.9%. This confirms the selective cytotoxicity of CEO against malignant cells. Additionally, for comparison, cells were incubated with two concentrations of doxorubicin (0.5 µM and 1 µM). The most affected cells were HeLa (56.0% viability), followed by HaCaT (69.1%); however, SiHa cells, which are generally more resistant to chemotherapeutic agents, were not affected and instead showed slightly accelerated proliferation.

Cinnamon essential oil triggers apoptosis through caspase- 8 and 9 activation following mitochondrial membrane depolarization.

Given our previous findings that CEO induces cell death, we further investigated the apoptotic mechanisms by assessing the activation of caspase-8 (extrinsic pathway), caspase-9 (intrinsic pathway), and caspase-3 (executioner caspase). Flow cytometry analysis was performed after 24 h of treatment with CEO at a 1:20,000 dilution.

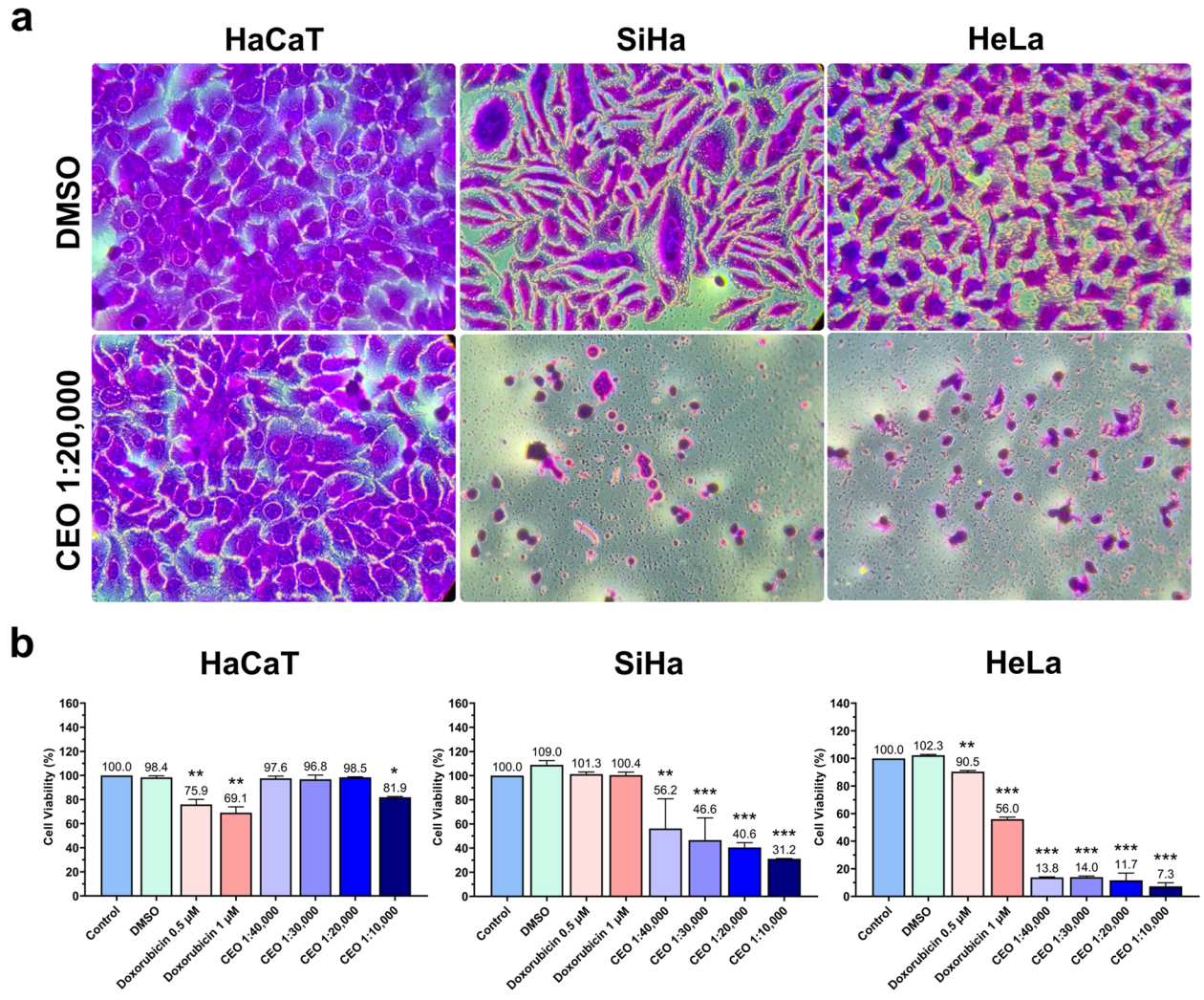


Fig. 3 Cell mass reduction observed under phase-contrast microscopy and cell viability assessed by Sulforhodamine B assay. **a** Representative phase-contrast micrographs (40×) of HaCaT, SiHa, and HeLa cells after 24 h of treatment with CEO at a 1:20,000 dilution or vehicle control (DMSO). **b** Measurement of total cellular protein content using sulforhodamine B (SRB) staining in HaCaT, SiHa, and HeLa cells. Cells were treated with increasing concentrations (1:40,000–10,000) of CEO, untreated (control), or DMSO (vehicle). Treatments with 0.5 or 1 µM doxorubicin were also included as positive controls. The results are expressed as the percentage of viable cells relative to the untreated control. Statistical significance is indicated as $^{*}p < 0.05$, $^{**}p < 0.01$, $^{***}p < 0.001$

As shown in Fig. 4a, CEO treatment resulted in a marked and statistically significant increase in the activation of all three caspases in the tumor-derived cell lines HeLa and SiHa compared to both untreated and vehicle-treated controls. In contrast, the nontumorigenic HaCaT cells showed no significant caspase activation, consistent with previous assays demonstrating minimal cytotoxic effects in this cell line. The marked activation of caspase-9 prompted us to examine whether CEO also affects mitochondrial integrity. Therefore, we evaluated changes in mitochondrial membrane potential (Δψm), a key indicator of mitochondrial function and a hallmark of apoptosis.

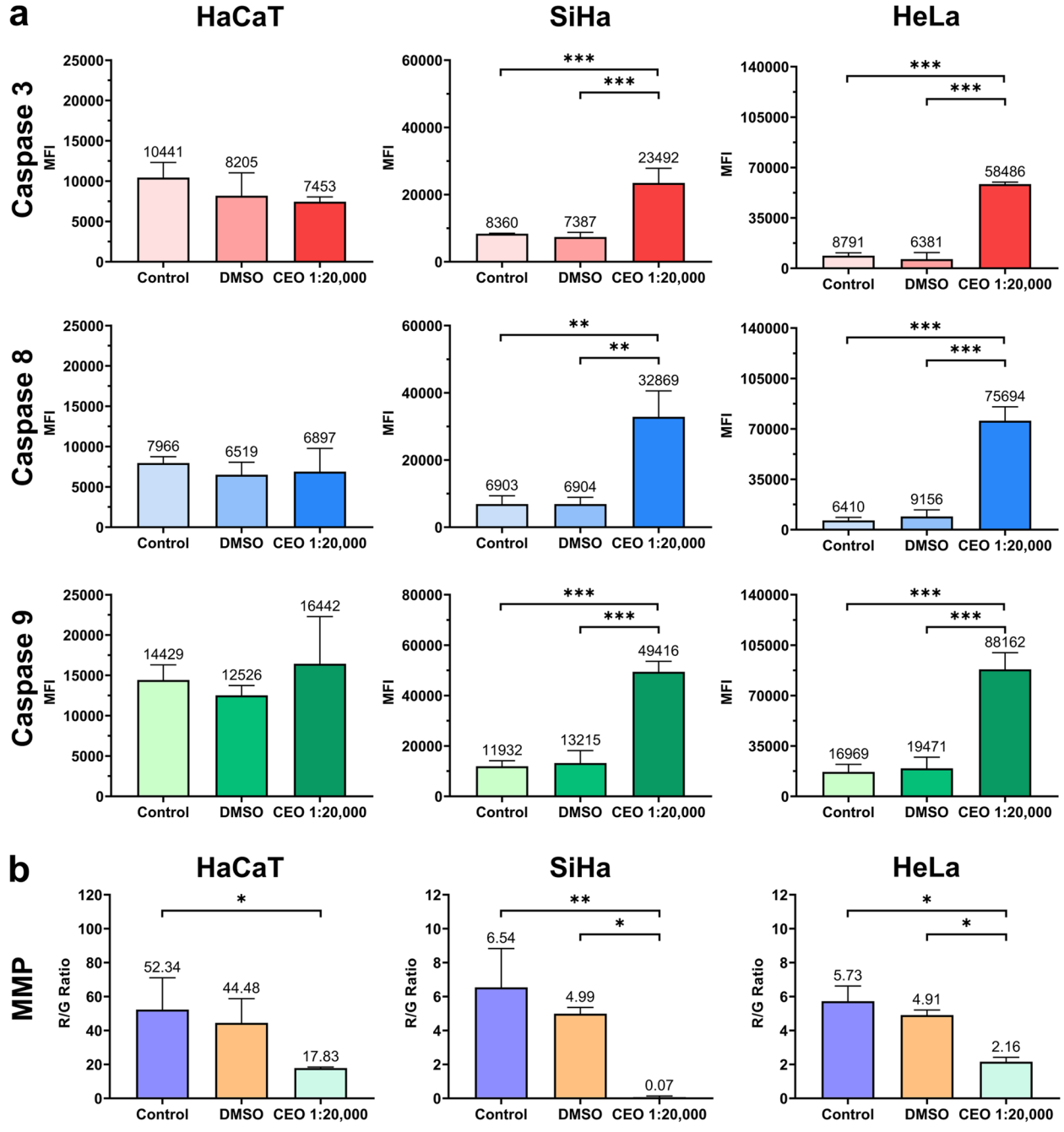


Fig. 4 Activation of caspases-3, –8, and –9 and assessment of mitochondrial membrane potential (ΔΨm). **a** Bar graphs represent the mean fluorescence intensity (MFI) of caspase-8 (extrinsic pathway), caspase-9 (intrinsic pathway), and caspase-3 (execution phase) measured by flow cytometry in HaCaT, SiHa, and HeLa cells after 24 h of exposure to CEO (1:20,000 dilution), untreated control, or DMSO (vehicle). Data are expressed as the mean ± SD from at least three independent experiments. **b** Bar graphs show the mitochondrial membrane potential (ΔΨm) assessed using JC-10 dye by flow cytometry. The graph displays the red (viable cells)/green (nonviable or late apoptotic) fluorescence intensity ratio, where a decrease in this ratio indicates a loss of ΔΨm. Statistical significance is indicated as $*p < 0.05$, $**p < 0.01$, $***p < 0.001$

As shown in Fig. 4b, Δψm was assessed using JC-10 dye after 24 h of CEO treatment. Healthy mitochondria emit red fluorescence, while depolarized mitochondria fluoresce green. CEO treatment caused a significant decrease in the red-to-green fluorescence ratio in HeLa cells from 5.73 (control) and 4.91 (DMSO) to 2.16 (CEO-treated cells; $p < 0.05$), indicating substantial mitochondrial membrane depolarization. SiHa cells showed a more profound drop from 6.54 (control) and 4.99 (DMSO) to just 0.07 in the CEO-treated cells ($p < 0.001$). Interestingly, in HaCaT cells, CEO treatment also induced a measurable reduction in the red/green ratio from 52.34 (control) and 44.48 (DMSO) to 17.83 in CEO (1:20,000 dilution).

The cytotoxic effect of cinnamon essential oil is mediated primarily by apoptosis rather than senescence

To evaluate cellular senescence induction, the mean fluorescence intensity (MFI) was measured by flow cytometry after 48 h of treatment with DMSO (vehicle), CEO (1:20,000), or doxorubicin (2 µM, positive control). In HaCaT cells, doxorubicin significantly increased MFI compared to the untreated control (143,782 vs. 68,951; $p < 0.05$), indicating strong senescence induction. In contrast, CEO caused only a modest, nonsignificant increase (MFI: 82,451). In SiHa cells, both CEO (558,930) and doxorubicin (685,500) increased MFI compared to the control (472,000). However, these changes were not statistically significant. Conversely, in HeLa cells, doxorubicin treatment significantly elevated MFI (78,679) compared to the control (23,485; $p < 0.05$), whereas treatment with CEO had no appreciable effect compared to the control or DMSO (25,973 vs. 23,485 or 18,964, respectively). Together, these results demonstrate that while the positive control doxorubicin consistently induced senescence, CEO did not produce a significant or consistent senescent response across cell lines (Fig. 5).

Cinnamon essential oil downregulates the expression of HPV oncogenes E6 and E7

Having established that CEO induces selective cytotoxicity, we next investigated its impact on the expression of the viral oncogenes *E6* and *E7* from HPV-16 and HPV-18, which are critical drivers of cervical carcinogenesis. Quantitative real-time PCR was performed to assess the mRNA levels of *E6* and *E7* in HPV-18-positive HeLa cells and HPV-16-positive SiHa cells following a 4-h treatment with CEO at a 1:20,000 dilution.

As shown in Fig. 6, CEO treatment resulted in a statistically significant downregulation of both *E6* and *E7* transcripts. In HeLa cells, expression levels were reduced to 0.83-fold for *E6* and 0.75-fold for E7 relative to DMSO controls ($p < 0.01$). A more pronounced downregulation was observed in SiHa cells, where CEO treatment decreased *E6* expression to 0.74 and E7 expression to 0.46 compared to controls ($p < 0.001$). These findings demonstrate the suppression of key HPV oncogenes, with a stronger inhibitory effect observed in SiHa cells.

Analysis of differentially expressed genes and enriched pathways following cinnamon essential oil treatment

To elucidate the molecular mechanisms of CEO, we performed transcriptomic profiling on the tumorigenic HeLa and SiHa cell lines and the nontumorigenic HaCaT keratinocytes. CEO exerted a strong modulatory effect on the transcriptome of all three cell lines. The volcano plot (Fig. 7a) illustrates the global transcriptomic landscape in gene expression following CEO treatment. Differentially expressed genes (DEGs) were defined by an adjusted p value (padj) < 0.05 and an absolute $\log_2$ fold

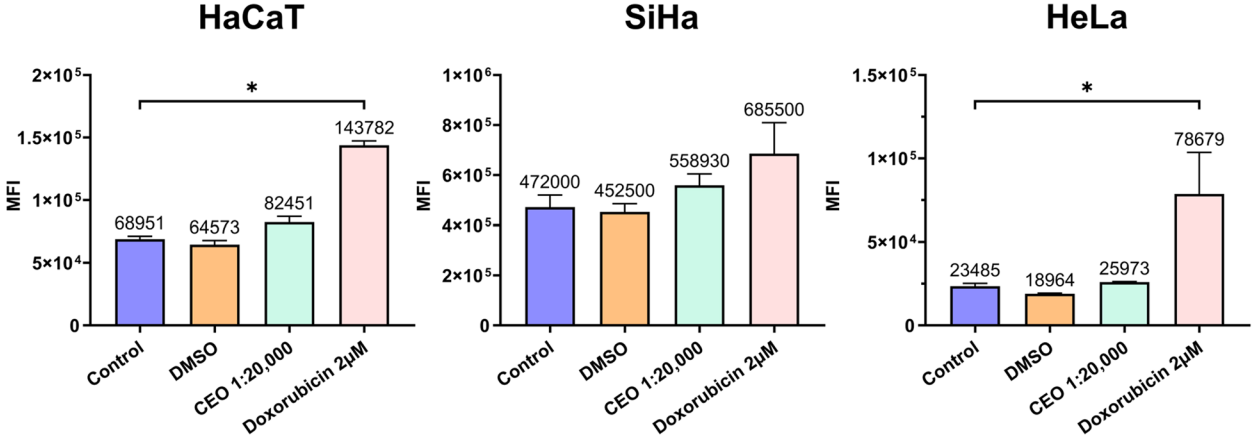


Fig. 5 Cellular senescence assessment using β-galactosidase (SA-β-gal) activity by flow cytometry. Bar graph plots depict the mean fluorescent intensity (MFI) of SA-β-gal–positive events in HaCaT, SiHa, and HeLa cells under four experimental conditions: untreated cells (Control), vehicle control (DMSO), cinnamon essential oil treatment (CEO 1:20,000), and a positive control (Doxorubicin) after 48 h of incubation. The results are expressed as the percentage of MFI ± SD from at least three independent experiments. Statistical significance is indicated as *$p < 0.05$

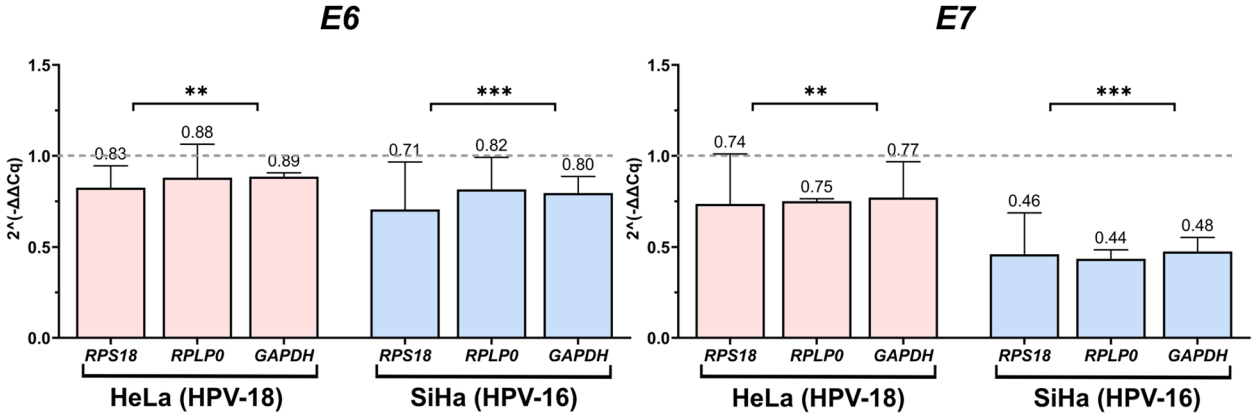


Fig. 6 Expression of HPV E6 and E7 oncogenes measured by qPCR. Bar graphs depict the expression levels of *E6* and *E7* in HeLa (red) and SiHa (blue) cells represented as 2^(-ΔΔCq). Normalization was performed using three reference genes (*RPS18*, *RPLP0*, and *GAPDH*). The dashed gray line indicates the expression level of the untreated cells (value set as = 1). Statistical significance is indicated as $^{**}p < 0.01$, $^{***}p < 0.001$

change ($|\log_2 FC| \geq 1.5$. This threshold was selected to identify genes with both statistical significance and biologically meaningful expression changes. In HeLa cells, the number of upregulated ($n = 172$) and downregulated ($n = 224$) genes were comparable. In contrast, SiHa and HaCaT cells displayed predominantly upregulated DEGs, with 426 up- and 206 downregulated DEGs and 615 up- and 340 downregulated DEGs, respectively.

The Venn diagram (Fig. 7b) summarizes the unique and shared DEGs among the cell lines. HeLa, SiHa and HaCaT cells exhibited 396, 632, and 955 total DEGs, respectively, with 176, 304, and 601 genes unique to each cell line. While 36 DEGs were shared exclusively between HeLa and SiHa and 62 between HeLa and HaCaT, a large overlap of 170 DEGs was observed between SiHa and HaCaT. A core of 122 DEGs were common across all three cell lines.

Figure 7c shows a heatmap of the 98 shared DEGs that remained after excluding noncoding genes and novel transcripts from the 122 common genes identified in the Venn diagram. To prioritize genes with the strongest response, DEGs were sorted by their fold change in HeLa cells, which were the most susceptible to CEO. This analysis revealed a core set of upregulated genes common to all cell lines, including *EGR2, FOSB, CHNRA2, EGR1*, *FOS, EGR3, RASD1, ARC, RND1, FOXJ1, MAFB, and COL2A1.* Notably, the expression changes of these shared DEGs were more moderate in SiHa cells. In contrast, HaCaT cells displayed the highest expression levels of some key stress response and apoptosis regulator genes, including *HMOX1, NR4A1*, *SNAI1*, *ASGR1, and RBFOX3,* while HeLa and SiHa cells showed comparatively moderate expression of these genes.

Cinnamon essential oil modulates pro-apoptotic, anti-proliferative, and stress-response pathways

To gain insights into the biological and molecular pathways impacted by CEO treatment, enrichment analysis was conducted using the Hallmark (GSEA) and KEGG (via PathFindeR) databases. Hallmark analysis (Fig. 8a) identified the top 20 significantly enriched pathways across the three cell lines. The commonly enriched pathways in the most CEO-sensitive HeLa and SiHa cells were TNFα signalling via NFκB, p53 signalling, UV response up, hypoxia, apoptosis, KRAS signalling up, mTORC1 signalling, and inflammatory response.

To strengthen the enrichment analysis, KEGG pathway analysis was also performed using PathFindeR (Fig. 8b). This approach confirmed the significant involvement of several key pathways common to the response, including TNF/NF-kappa B signalling, mTOR signalling, the p53 pathway, cell cycle regulation, cellular senescence, and apoptosis. However, the enrichment of certain pathways varied across cell lines. In HaCaT cells, the most significantly enriched KEGG pathways included the longevity regulating pathway, inositol phosphate metabolism, and collecting duct acid secretion. In SiHa cells, enrichment was prominent in pathways related to Type II diabetes mellitus, Autophagy, and the Circadian rhythm and in HeLa Legionellosis, p53 signalling, and apoptosis.

Predicted Protein–protein Interaction (PPI) network analysis

To explore functional interactions among the 98 filtered shared DEGs, protein–protein interaction (PPI) networks were constructed using the STRING database. For the subsequent protein-protein interaction network analysis, we applied a medium confidence score (0.4) to focus on relevant nodes and excluded disconnected nodes. The resulting network (Fig. 9) revealed 58 connected nodes with three major clusters: one composed of transcriptional regulators (*FOS*, *FOSB*, *JUN*, *EGR1*, *EGR2*, *EGR3*, *DUSP1*, and *ATF3)* associated with cellular stress, proliferation, and autophagy; a second cluster containing DNA damage response genes (*GADD45B*, *SOCS3*, *DUSP5*,

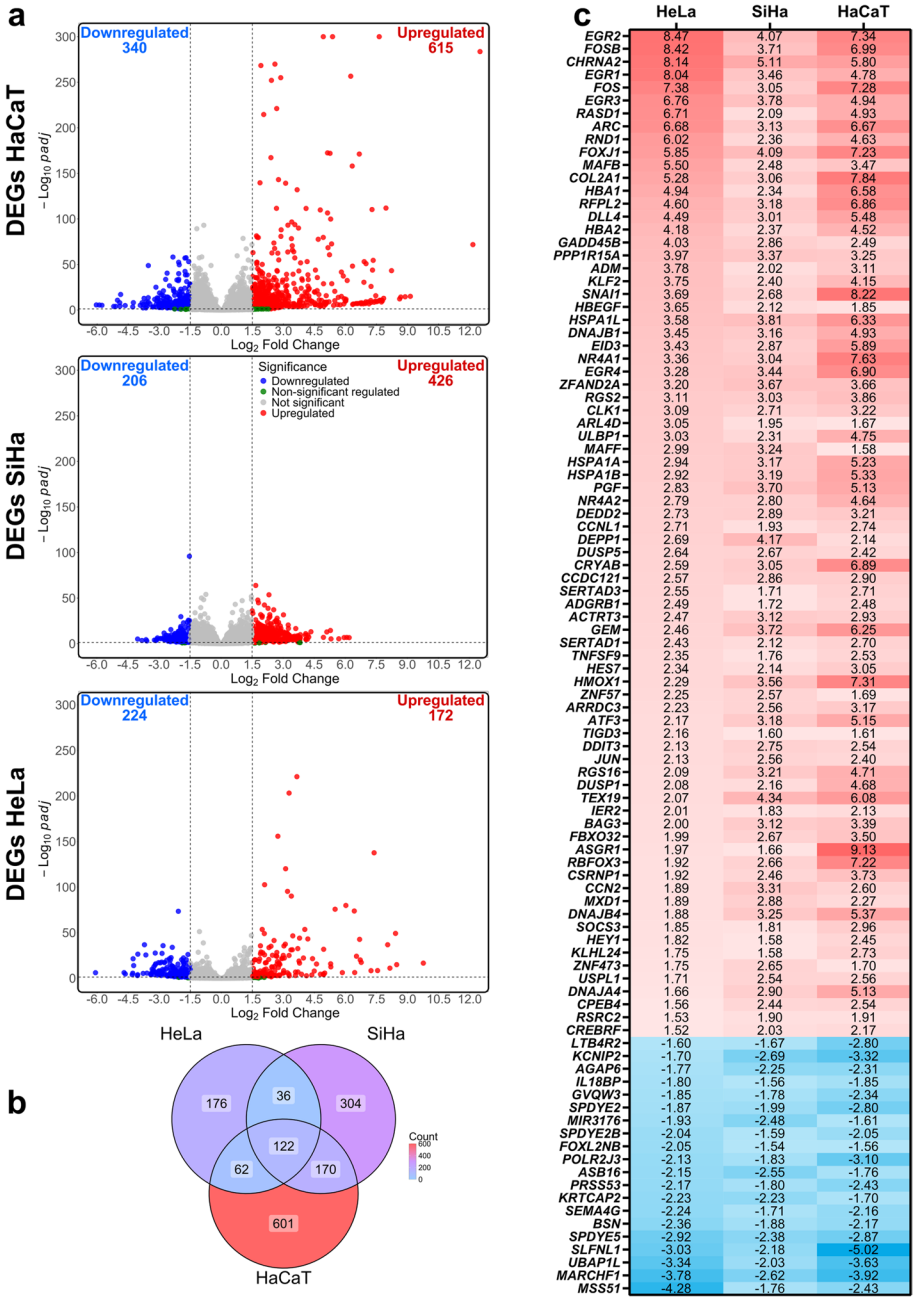


Fig. 7 Transcriptomic analysis of CEO-treated cells. **a** Volcano plots showing differentially expressed genes (DEGs) in HaCaT, SiHa, and HeLa cell lines. Upregulated genes are shown in red, downregulated genes in blue, and nonsignificant genes in gray. The total number of DEGs identified in each cell line is indicated below each plot. The x-axis represents the log2-fold change, and the y-axis shows the –log10 adjusted *p* value. Each dot represents a single gene. **b** Venn diagram depicting the unique and shared DEGs among the three cell lines. Color intensity represents the number of DEGs (red = higher number, blue = lower number). **c** Heatmap of the 98 commonly regulated DEGs across all cell lines, displaying log2-fold change values included. Red indicates upregulation, and blue indicates downregulation. These 98 DEGs corresponded to the 122 genes from the Venn diagram after filtering out noncoding genes and novel transcripts. Additional file 1 provides a broader overview of the top differentially expressed genes (both upregulated and downregulated) in each cell line

DDIT3, and *PPP1R15A)* and a putative tumor suppressor gene (*CSRNP1*); and a third cluster related to ER stress and protein folding, featuring *HSPA1A*, *HSPA1B*, *HSPA1L*, *DNAJA4*, *DNAJB1*, *DNAJB4*, *CRYAB*, and *HMOX1*. Additional file 2 further extends these findings by illustrating the PPI networks generated independently for each cell line based on their respective top 50 upregulated and downregulated genes.

To gain deeper insight into the mechanisms driven by CEO treatment, we determined the genes and pathways

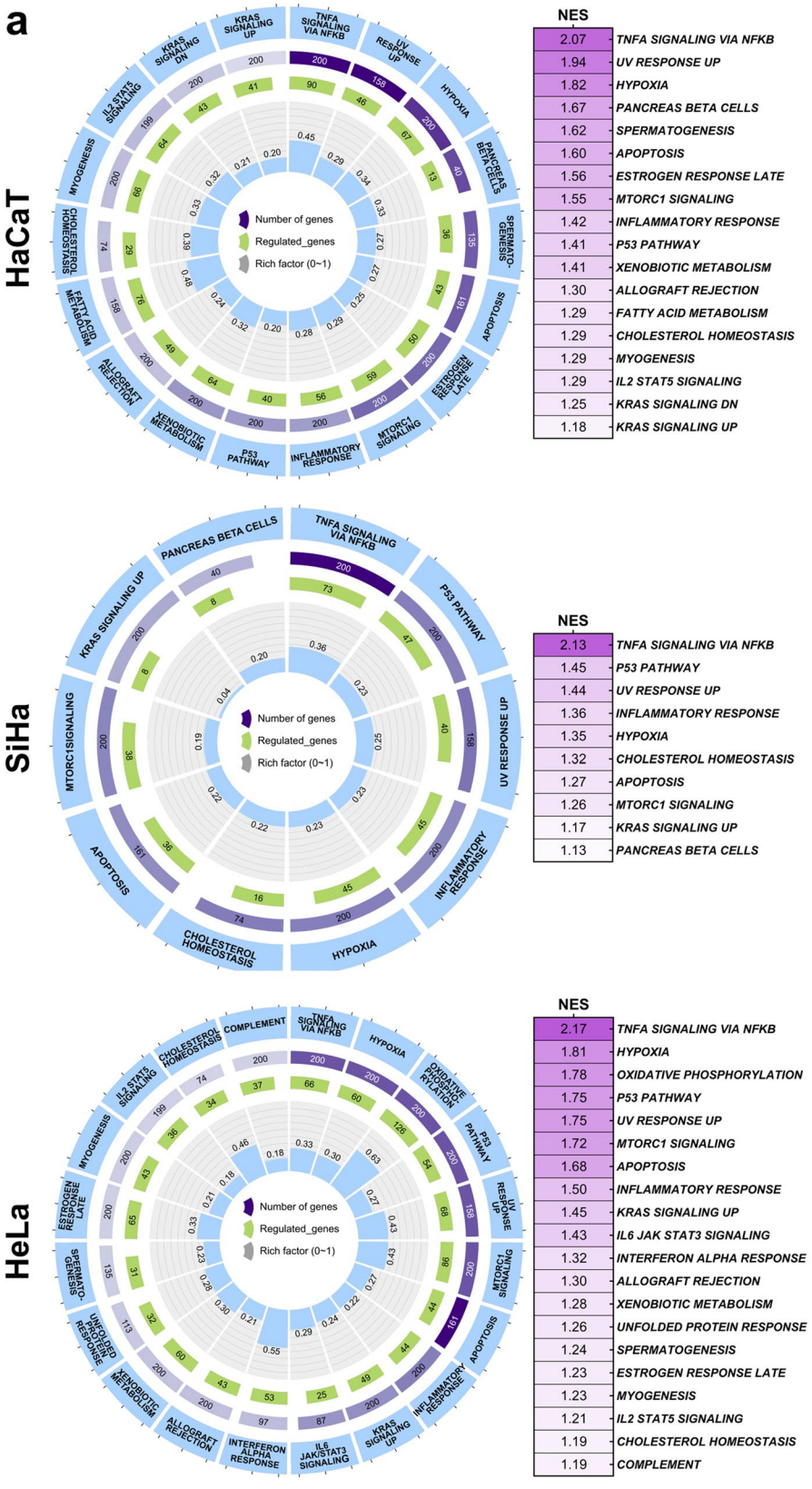


Fig. 8 (See legend on next page.)

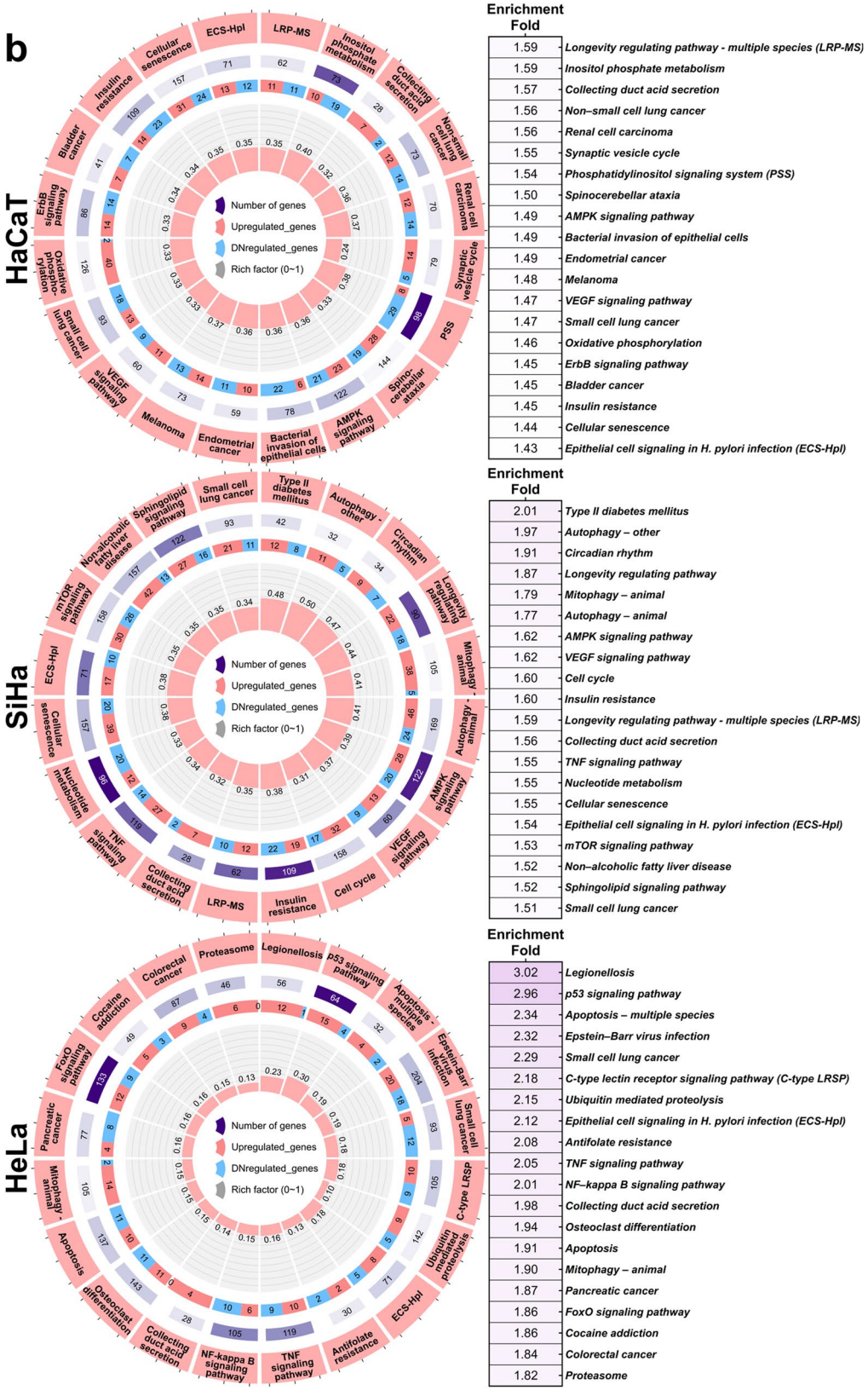


Fig. 8 (continued)

(See figure on previous page.)

Fig. 8 Enriched pathways from (**a**) hallmark and (**b**) KEGG pathway analyses. Polar plots illustrate the enriched pathways in the outer ring, along with the total number of genes associated with each pathway. Color intensity represents statistical significance. The subsequent ring indicates the number of enriched genes. The inner ring denotes the rich factor, calculated as the ratio of enriched genes relative to the total number of genes within the pathway. On the right, heatmaps display the NES (normalized enrichment score) in hallmark analyses or the enrichment fold for KEGG analyses. Color intensity reflects the degree of enrichment, and the numeric values within each cell indicate the enrichment score for the corresponding pathway

that were most significantly modified, particularly in each cell line. As shown in Fig. 10, the STRING-derived network diagram illustrates the differential up- and down- regulated biological processes and signalling pathways modulated by CEO in HeLa, SiHa, and HaCaT cells.

In HeLa cells, the primary upregulated processes were strongly associated with stress response (*CXCL3*, *IER3*), cell fate (*AXIN2*, *DLL1*) and angiogenesis (*COL18A1*, *PECAM1*), while those downregulated were linked to cell proliferation/survival (*DICER1 HOXC8*, *MRNIP*, *CDK6*) and cell signalling (*WFIKKN1*, *UBASH3B*, *KCNAB3*). Of notable interest was the substantial proportion of mitochondrial genes that were preferentially downregulated (such as *MT-CO1*, *MT-CO2*, and *MTCO2P12*).

The SiHa cell line exhibited a different regulatory profile. Upregulated pathways and genes with the highest edge confidence involved regulation of neutrophil migration (*CXCL8*, *IL1A,* and *TNFAIP6*), cell plasticity/stress (*MYC*, *SOX9*, *SNAI1*), regulation of T-helper 2/cell cytokine production (*GATA3*, *TBX21*), and endothelial cell apoptotic processes (*PCK1*, *ANGPTL4*). Conversely, the downregulated processes in SiHa cells focused on the netrin-activated signalling pathway (*NTN* −1, −3, *IGDCC4*), benzodiazepine receptor binding (*RIMBP3*, *RIMBP3B*, *RIMBP3C*), a domain of unknown function DUF4074 (*HOXD4*, *HOXD9*), and stemness-maintaining programs (*DKK1*, *ID1*).

On the other hand, in the nontumorigenic HaCaT keratinocytes, the response was distinct. One prominent cluster corresponded to interleukin-6 family signalling, centered on IL6. A second major subnetwork was enriched for components of the TNFR1-induced NF-κB signalling pathway, with UBB acting as a central hub. Additionally, a distinct cluster was associated with autophagy (*MAP1LC3A*, *ATG4A*, *GABARAPL1*, etc.), and a smaller cluster was related to the cyclin-dependent protein kinase holoenzyme complex (*CCNA1*, *CCNE1*, *CKS2*, *FBXW7*). The downregulated processes in HaCaT included mitogen (*TGFA*, *PDGFB*, *IL3RA*, *LIF*), keratinization (*LCE1E*, *SPRR2A*, *SPRR2D*, *SPRR2E*), inhibition of voltage-gated Ca^{2+} channels via Gβ/γ subunits (*GABBR1*, *GNG13*, *DRD4*), and calcium-mediated stress response (*TRPV1*, *ADCY6*, *CALML6*).

qPCR analysis confirms the transcriptomic profile induced by cinnamon essential oil

Finally, to validate the transcriptomic findings obtained by RNA-seq following CEO treatment, quantitative real-time PCR (qPCR) was performed on 19 selected genes from different clusters, including *EGR1*, *GADD45B*, *PPP1R15A*, *SNAI1*, *PGF*, *HMOX1*, *ATF3*, *DDIT3*, *JUN*, *SOCS3, KLHL24, CDKN1A*, *CCND1*, *MTCO1*, *MTCO2*, *MTCO3*, and *MTCO2P12*. As depicted in Fig. 11, the upregulation or downregulation of all selected genes was validated by these assays, with concordant trends observed between the RNA-seq and qPCR data.

Discussion

The present study provides a comprehensive analysis of the ability of cinnamon essential oil (CEO) to induce selective cytotoxicity, mitochondrial-mediated apoptosis, suppression of HPV oncogene expression, and modulation of key transcriptomic pathways. While previous studies have demonstrated the anticancer effects of cinnamon extracts or cinnamaldehyde in various cancer models, including cervical cancer cells [44, 45], our study provides several novel contributions to the field. First, to our knowledge, this is the first comprehensive transcriptomic analysis (RNA-seq) of CEO-treated cervical cancer cells, offering a genome-wide view of the molecular pathways modulated by this natural product. Second, we demonstrate that CEO simultaneously suppresses HPV *E6*/*E7* oncogene expression while inducing mitochondrial dysfunction, a dual mechanism that has not been previously characterized in HPV-positive cervical cancer models. Third, our comparative analysis of tumorigenic (HeLa, SiHa) and nontumorigenic (HaCaT) cells yields novel insights into the selective cytotoxicity of CEO and the potential protective mechanisms in normal cells (e.g., *HMOX1* upregulation). Fourth, the identification of core transcriptional programs shared across cell lines, encompassing stress response and DNA damage pathways, establishes a molecular framework for understanding CEO's mechanism of action.

Thus, our findings demonstrate that low concentrations of CEO exert a potent and selective cytotoxic effect against cervical cancer cell lines (HeLa and SiHa), while the nontumorigenic HaCaT cells were affected to a much lesser extent, as evidenced by WST-1, Annexin V/PI, and SRB assays (Figs. 1, 2 and 3).

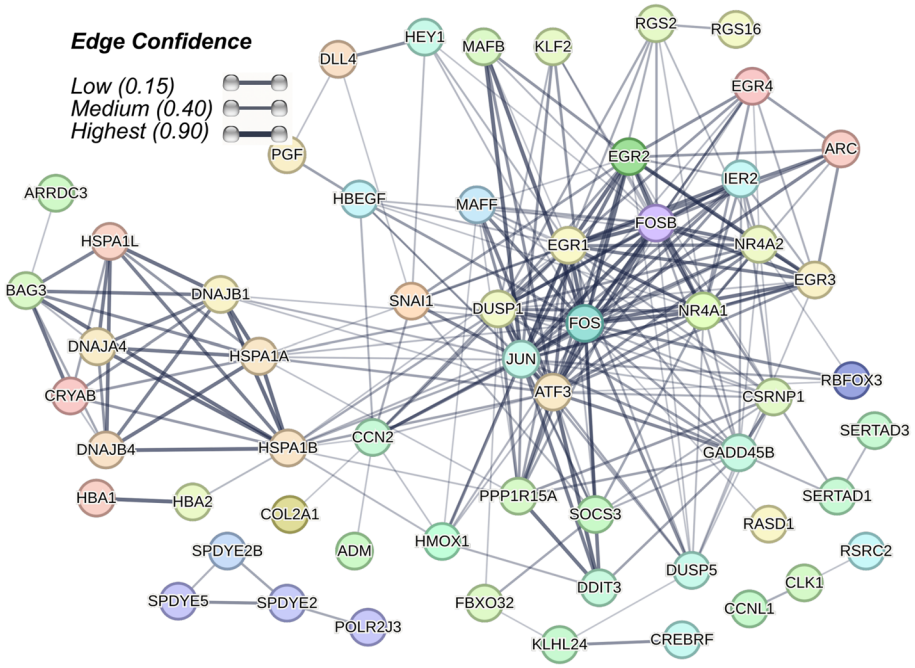


Fig. 9 Protein–protein interaction network of the 98 filtered DEGs shared among HaCaT, SiHa, and HeLa cells. The PPI network interaction was generated using the STRING database to visualize functional associations among the gene products. It comprises 58 connected nodes, each representing a gene product, while edges denote pairwise interactions. Edge thickness reflects the confidence score of each interaction based on curated experimental data, coexpression analyses, and scientific literature

These results align with previous reports demonstrating the anti-neoplastic activity of cinnamon extracts against cervical cancer cells, including those observed in HeLa cells [44]. Koppikar et al. [45] reported that aqueous cinnamon extract from *Cinnamomum cassia* induced apoptosis in SiHa cells through loss of mitochondrial membrane potential. Additionally, these results are consistent with previous reports showing that CEO (*Cinnamomum zeylanicum*) preferentially targets malignant cells (MCF7, T47D, MDA-MB-231, K562, SH-SY5Y, HCT116, and fibroblasts transformed by *c-Ha-ras* oncogene 5RP7 cells) while sparing noncancerous cells, such as the human fetal lung fibroblast MRC-5 cell line or normal F2408 fibroblasts [28, 30, 46]. Moreover, *Cinnamomum zeylanicum* showed a significant chemopreventive effect in a model of chemically induced mammary carcinogenesis in rats and a significant therapeutic effect in a 4T1 adenocarcinoma model in mice [32].

The differential sensitivity observed between tumorigenic and nontumorigenic cells may reflect intrinsic differences in metabolic activity or oxidative stress responses. As has been reported in many reviews, cancer cells often exhibit higher basal levels of reactive oxygen species (ROS) and are therefore more susceptible to further oxidative insults induced by phytochemicals [47], a mechanism by which many therapies selectively kill cancer cells through ROS induction [48–50]. Furthermore, cinnamaldehyde, the main component of CEO, has been reported to trigger apoptotic signalling and/or disrupt mitochondrial function in the colon cancer cells HCT116, HT-29, SW480, and LoVo [51, 52], in the hepatocellular carcinoma HepG2 cells [53], and in the breast cancer MDA-MB-231 cells [54], which could explain the pronounced apoptotic effect in HeLa and SiHa cells.

Mechanistically, our data demonstrated that CEO-induced cell death occurs primarily through the intrinsic mitochondrial apoptotic pathway, as evidenced by significant activation of caspase-9 and loss of mitochondrial membrane potential ($\Delta\psi m$) measured by JC-10 (Fig. 4). These findings are consistent with previous studies reporting that cinnamon extracts or their bioactive components, such as cinnamaldehyde, can compromise mitochondrial integrity and promote cytochrome c release, ultimately leading to apoptosis. This has been observed in SiHa cells [45], the human colon cancer-derived HCT-116 cell line [55], prostate cancer-associated fibroblasts [40], human leukemia HL-60 and K562 cells [36, 56], and glioblastoma-derived U87MG cells [57]. Additionally, *Cinnamomum zeylanicum* and cinnamaldehyde have been shown to induce apoptosis in oral cancer cell lines SCC-4, SCC-9, and SCC-25 [58]. Beyond the glioblastoma model, cinnamaldehyde has been shown to act synergistically with oxaliplatin in colorectal cancer [38], with paclitaxel in breast cancer via PI3K/AKT modulation, and with cisplatin in resistant cervical cancer cells through ROS-mediated apoptosis. These findings suggest

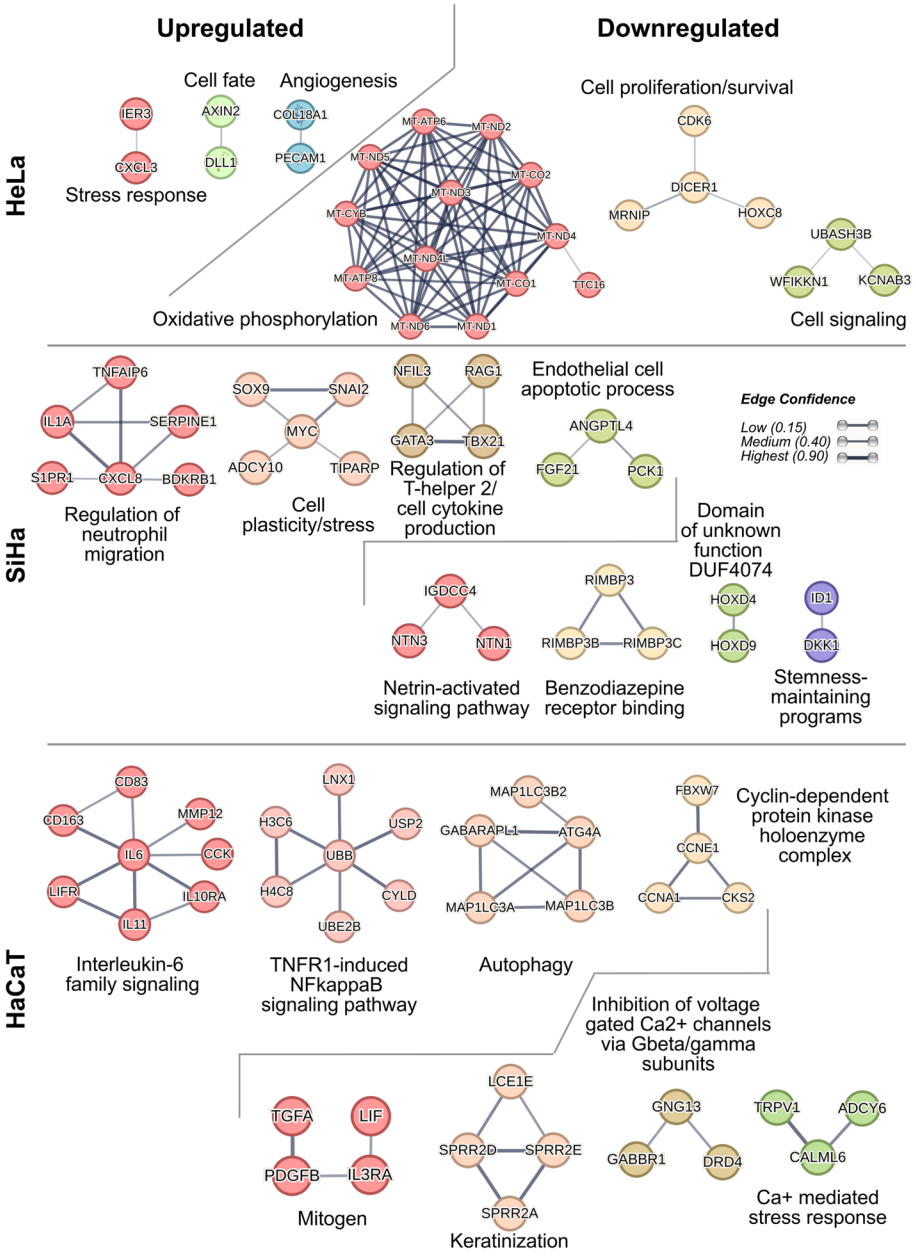


Fig. 10 Functional clusters derived from protein–protein interaction network analysis of upregulated and downregulated genes. PPI networks were constructed from DEGs using the STRING database and analysed with the Markov cluster algorithm (MCL) to identify highly interconnected functional modules. The main clusters associated with upregulated and downregulated genes in each cell line are shown comparatively. Edge confidence levels (low = 0.15, medium = 0.40, highest = 0.90) are represented by line thickness, indicating the strength of supporting evidence for each interaction

that CEO or its components could function as chemosensitizers, warranting further investigation into combination strategies for HPV-positive cervical cancer.

The EdU incorporation and SRB assays further confirmed the antiproliferative effect of CEO, with significant reductions in DNA synthesis and significant protein loss observed specifically in HeLa and SiHa cells (Figs. 2 and 3). These results are in line with other studies reporting reduced proliferation following treatment with CEO, its main component cinnamaldehyde, or other cinnamon species, such as *Cinnamomum cassia*. Using BrdU incorporation assays, similar antiproliferative effects were observed in the breast cancer-derived MCF-7 and MDA-MB-231 cell lines [32]. The relative resistance of HaCaT cells, along with their slight increase in proliferation, suggests that CEO may exert context-dependent effects based on the cellular metabolic or signalling landscape. Such selectivity could represent an advantage over conventional chemotherapeutics, which often lack discrimination between malignant and nonmalignant cells.

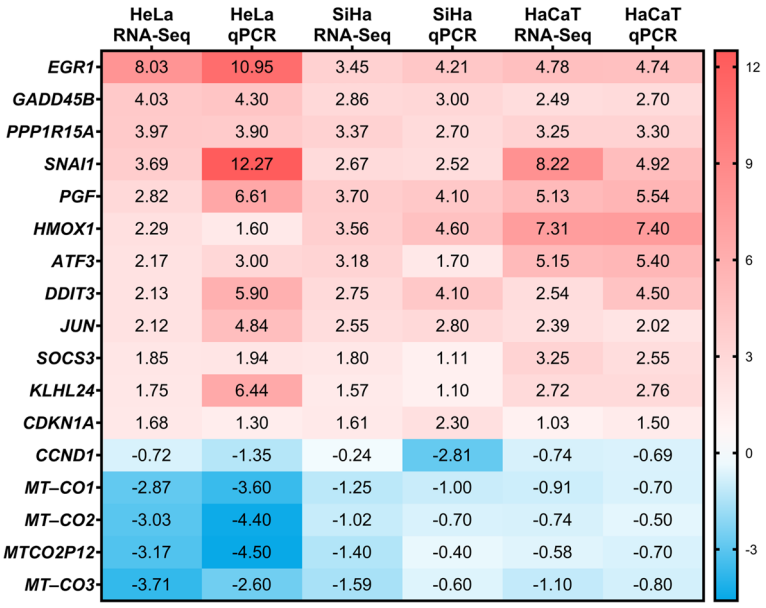


Fig. 11 Validation of selected gene expression changes by qPCR. Heatmap displaying the expression data of 17 selected genes across HeLa, SiHa, and HaCaT cell lines following CEO treatment (1:20,000). Red boxes indicate upregulation, and blue boxes indicate downregulation, represented as Log_2FC values obtained from both RNA-seq and qPCR analyses. Gene names are listed on the right, while the top axis indicates the respective cell line and analysis type (RNA-seq or qPCR)

Notably, doxorubicin did not elicit a significant antiproliferative response in SiHa cells (Fig. 3B). This may be attributed to the differential chemosensitivity known to exist across cervical cancer cell lines at the concentrations tested (0.5–1 μM). Multiple studies have reported that SiHa cells are generally more resistant than HeLa cells to various chemotherapeutic agents: Venkatraman et al. directly demonstrated that SiHa cells were relatively more resistant to cisplatin-induced cytotoxicity than HeLa cells, showing reduced apoptotic markers and caspase activation [59]; Filippova et al. employed SiHa cells as a model of resistance to doxorubicin and cisplatin, identifying elevated antioxidant enzyme expression as a contributing mechanism [60]; and León et al. established differential sensitivity profiles across cervical cancer cell lines, including SiHa and HeLa, when exposed to doxorubicin, Taxol, and cisplatin [61]. Taken together, these findings suggest that the concentration used may have been suboptimal for SiHa cells, which may require higher doses to elicit significant cytotoxic effects.

The evaluation of cellular senescence in this study was crucial to further characterize the biological effects of CEO beyond apoptosis and proliferation arrest. Senescence is a stable cell cycle arrest that can act as a tumor-suppressive mechanism by halting the proliferation of damaged or transformed cells [62, 63]. However, persistent senescent cells may acquire a senescence-associated secretory phenotype (SASP), releasing proinflammatory cytokines, growth factors, and proteases that remodel the tissue microenvironment and can paradoxically promote tumor progression, chronic inflammation, and therapy resistance [64]. Thus, while the induction of senescence may limit immediate tumor growth, it also carries potential long-term risks [65]. In this context, we observed that CEO did not robustly induce senescence, particularly in highly sensitive HeLa cells, while doxorubicin consistently triggered senescence across all tested cell lines (Fig. 5). CEO showed only modest, cell type-dependent effects, with partial induction observed in HaCaT and SiHa cells. These findings suggest that CEO and doxorubicin inhibit cancer cell growth through distinct mechanisms. While doxorubicin primarily acts by inducing DNA breaks and inhibiting topoisomerase II activity [66], CEO may exert its effects indirectly through oxidative stress-mediated damage, potentially independently of the senescence pathway. Alternatively, the rapid induction of apoptosis could preclude senescence development in more sensitive cells such as HeLa cells. This feature is therapeutically advantageous, as it reduces the likelihood of SASP-related adverse effects and indicates that CEO eliminates cancer cells more definitively via apoptosis rather than inducing a reversible or potentially harmful latent state. Consequently, this property enhances the appeal of CEO or its bioactive components as candidates for further development into novel anticancer agents.

A particularly significant finding of our study is the downregulation of HPV oncogenes *E6* and *E7* following CEO treatment, with a more pronounced effect observed in SiHa cells (Fig. 6). These results are remarkably consistent with a very recent study published in 2025, which

demonstrated that cinnamaldehyde induces degradation of both oncoproteins [67]. The alignment of our findings with this newly elucidated mechanism validates our observations and suggests that E6/E7 suppression may contribute to apoptosis in HPV-positive cervical cancer cells, alongside the mitochondrial dysfunction and stress pathway activation already discussed. It is worth noting that the transcriptional downregulation of *E6* and *E7*, while statistically significant, was relatively modest, particularly in HeLa cells. Protein-level validation would offer stronger evidence but remains technically challenging, given the well-documented limitations of commercially available antibodies for detecting endogenous E6 and E7, including poor sensitivity, cross-reactivity with cellular proteins [68], and the inherent lability and rapid turnover of the E6 protein [69, 70]. Future studies employing coimmunoprecipitation or targeted mass spectrometry-based proteomics could help overcome these limitations.

The RNA-seq analysis performed in our study provides a comprehensive overview of the global molecular response to CEO in cervical cancer cells (Figs. 7, 8, 9, and 10). The enrichment of TNFα signalling via NFκB, the p53 pathway, hypoxia, and apoptosis in hallmark analysis, together with KEGG pathway enrichment for TNF/NF-kappa B signalling, mTOR signalling, and the p53 pathway, indicates that CEO affects multiple proapoptotic and stress-responsive signalling cascades. Consistent with our observations, recent studies have confirmed that these pathways are modulated by treatment with cinnamon essential oil or its bioactive components [71, 72].

In addition, a core set of 122 common DEGs emerged across all cell lines after CEO treatment. Regarding the analysis performed with STRING (Fig. 9), prominent clusters were identified, including transcriptional regulators (*EGR1*, *EGR2*, *FOS*, *JUN*) [73, 74], stress responders (*HMOX1*, *HSPA* family, *DNAJ* family) [75–77], and genes involved in the DNA damage response (*GADD45B*, *DDIT3*, *PPP1R15A*) [78–80]. This profile suggests that CEO triggers broad cellular stress programs that converge on apoptosis execution specifically in cancer cells.

Concerning the individual genes found to be commonly down- or upregulated, one that particularly drew our attention was the strongly upregulated expression of *HMOX1* in the HaCaT cell line, observed consistently in both RNA-seq and qRT−PCR validation assays (Figs. 7, 8, 9, 10 and 11). This observation aligns with reports linking cinnamaldehyde to the induction of *HMOX1* expression in human keratinocytes [81]. *HMOX1* encodes an enzyme that plays a key role in the cellular antioxidant response [82]. Given that HaCaT cells exhibited the highest resistance to CEO treatment, it is plausible that cinnamaldehyde triggered a protective antioxidant effect in these cells, which may account for their higher resistance.

Conversely, we observed a strong downregulation of *MT-CO1*, *MT-CO2*, and *MT-CO3*, particularly in HeLa cells (Fig. 11). These core components of mitochondrial complex IV [83] are essential for driving oxidative phosphorylation, the process that generates the vast majority of cellular ATP. This transcriptional repression effectively disrupts the cell´s primary energy source, aligning with the oxidative phosphorylation enrichment detected in KEGG pathways and the loss of mitochondrial membrane potential observed in functional assays. Collectively, these results indicate that CEO compromises mitochondrial bioenergetics. Additionally, trans-cinnamaldehyde has been reported to protect against oxidative stress, ROS, and mitochondrial damage in nontumorigenic C2C12 mouse cells [84]. These findings are consistent with our results in the nontumorigenic HaCaT model, where no damage was observed and minimal downregulation of mitochondrial genes was observed.

On the other hand, the downregulated genes *SLFNL1*, *MSS51*, *SPDYE2B*, *SPDYE5B*, *SPDYE5*, *SLFNL1*, *UBAP1L*, and *MARCHF1* stand out due to their key roles in cellular homeostasis. *MSS51* acts as a mitochondrial translational activator essential for respiratory chain gene expression and mitochondrial integrity [85], while members of the Speedy/RINGO family (*SPDYE2B*, *SPDYE5B*, *SPDYE5*) regulate cyclin-dependent kinase (CDK) activity, influencing cell cycle progression and the response to antiproliferative signals [86]. Together, these genes may link mitochondrial function with cell cycle control, reflecting coordinated regulation between metabolism and proliferation. This is consistent with the enrichment of oxidative phosphorylation and cell cycle pathways observed in both the hallmark and KEGG analyses. By reducing the expression of these cell cycle drivers, CEO treatment may slow or halt cell division, a key mechanism underlying its potential anticancer properties.

Although our transcriptomic analysis pointed to oxidative stress, as evidenced by the upregulation of *HMOX1* and HSPA family genes and the enrichment of TNFα/NF-κB signalling, direct measurement of ROS levels was not performed in this study. DCFH-DA-based quantification would clarify whether ROS production is a primary driver of CEO-induced cytotoxicity or a secondary consequence of mitochondrial dysfunction. Future studies incorporating both ROS quantification and antioxidant rescue experiments are warranted to further elucidate this mechanism.

Several studies have evaluated the in vivo anticancer potential of cinnamon extracts or their major bioactive component, cinnamaldehyde. Kubatka et al. [32] demonstrated that *Cinnamomum zeylanicum* bark extract exhibited significant chemopreventive efficacy in a rat model of chemically induced mammary carcinogenesis and therapeutic effects in a 4T1 adenocarcinoma mouse

model. Additionally, cinnamaldehyde has been shown to inhibit tumor growth and metastasis in various xenograft models, including colorectal cancer [38], hepatocellular carcinoma, and melanoma. However, these studies are limited by variable extract compositions, lack of standardized dosing, and limited pharmacokinetic data. The translation of these findings to cervical cancer models, particularly HPV-driven tumors, remains unexplored, highlighting the need for future in vivo studies using well-characterized CEO preparations and appropriate HPV-positive tumor models.

Moreover, regarding safety, cinnamon extracts and cinnamaldehyde have generally shown favourable toxicity profiles in animal models. Oral administration of cinnamaldehyde at doses up to 500 mg/kg/day in rodents has been well tolerated, with no significant organ toxicity observed in subchronic studies [87]. In humans, although moderate consumption of cinnamon-containing foods or supplements may confer health benefits, excessive intake could trigger herb drugs via PXR or AhR activation [88], and adverse events have been documented in clinical trials [89–93], raising concerns for individuals with chronic conditions. For topical applications, essential oils may cause skin irritation at high concentrations [94]. These safety considerations underscore the importance of careful dose optimization and formulation development for potential therapeutic applications. Finally, it should be noted that the chemical composition of essential oils can vary depending on the plant source, extraction method, and batch. While we used a commercially available, standardized CEO preparation with a reported composition, independent GC–MS characterization in future studies would enhance reproducibility and help identify the specific bioactive components responsible for the observed effects.

Conclusion

In conclusion, CEO exhibits potent and selective antitumour activity against HPV-positive cervical cancer cells in vitro through a multifaceted mechanism that integrates the suppression of viral oncogenesis with the disruption of cellular metabolism and stress responses. Specifically, CEO triggers mitochondria-mediated apoptosis (evidenced by caspase activation and ΔΨm loss) and downregulates HPV E6/E7 oncogene expression (as confirmed by qPCR). Transcriptomic and enrichment analyses reveal robust signatures for apoptosis, oxidative phosphorylation, protein processing in the endoplasmic reticulum, and cell cycle/senescence regulation, alongside reprogramming of pathways governing proliferation, stress adaptation, and energy metabolism, including p53, TNFα/NF-κB, and mTORC1 signalling. However, further functional studies are required to confirm causality and the direct involvement of these pathways in CEO-mediated effects. The multitarget nature of CEO may offer advantages over single-target therapies. Nevertheless, it should be emphasized that these findings are derived from in vitro experiments using established cell lines. Future studies using appropriate in vivo models, including xenograft and genetically engineered mouse models, as well as primary patient-derived samples, are essential to validate the anticancer activity of CEO and its bioactive components, evaluate pharmacokinetics and bioavailability, and assess potential toxicity and therapeutic safety profiles.

Altogether, the coordinated upregulation of stress- and apoptotic-related genes, coupled with the downregulation of mitochondrial transcripts, reinforces the conclusion that CEO acts through an integrated disruption of oncogenic signalling and metabolic homeostasis, providing a strong rationale for further preclinical development.

Abbreviations

AV	Annexin V
CC	Cervical cancer
CEO	Cinnamon essential oil
DEG	Differentially expressed gene
DMEM	Dulbecco's Modified Eagle Medium
DMSO	Dimethyl sulfoxide
EdU	5-Ethynyl-2'-deoxyuridine
FBS	Foetal bovine serum
FC	Fold change
GSEA	Gene Set Enrichment Analysis
HPV	Human papillomavirus
IC_{50}	Half-maximal inhibitory concentration
KEGG	Kyoto Encyclopedia of Genes and Genomes
MFI	Mean fluorescence intensity
MMP	Mitochondrial membrane potential
NES	Normalized enrichment score
PBS	Phosphate-buffered saline
PI	Propidium iodide
PPI	Protein–protein interaction
qPCR	Quantitative polymerase chain reaction
RIN	RNA integrity number
RNA-seq	RNA sequencing
ROS	Reactive oxygen species
SASP	Senescence-associated secretory phenotype
SD	Standard deviation
SRB	Sulforhodamine B
WHO	World Health Organization
ΔΨm	Mitochondrial membrane potential

Supplementary Information

The online version contains supplementary material available at https://doi.org/10.1186/s12906-026-05471-7.

Supplementary Material 1.

Supplementary Material 2.

Acknowledgements

R.P.-C (CVU 1182601), A.M.-P. (CVU 813683), S.V.-R. (CVU 1171667), and J. G.-G. (CVU 1256380) are grateful for scholarships from the Secretariat of Science, Humanities, Technology and Innovation (SECIHTI)- Mexico. The English language in this manuscript was corrected and improved using the artificial intelligence tool DeepSeek (https://chat.deepseek.com/) and Rubriq (https://rubriq.com/).

Authors' contributions
Conception, A.A.-L., L.F.J.-S., R.H.-G., M.G.-C; Design of the work, A.A.-L., L.F.J.-S., R.H.-G., M.G.-C; Acquisition, A.A.-L.; Analysis, R.P.-C, A.M-P., J.G.-G., S.V.-R.; Interpretation of data, R.P.-C, A.M-P., J.G.-G., S.V.-R.; Visualization, R.P.-C, A.M-P., J.G.-G., S.V.-R.; Original draft, R.P.-C. and A.M-P.; Substantively revision of the manuscript, A.A.-L., L.F.J.-S., R.H.-G., M.G.-C. All the authors have read and approved the submitted version of the manuscript and have agreed both to be personally accountable for the author's own contributions and to ensure that questions related to the accuracy or integrity of any part of this work.

Funding
This work was supported by the ***Instituto Mexicano del Seguro Social*** (IMSS) through Grant No. R-2024–1305-054, awarded to A.A.-L.

Data availability
The data sets generated and analyzed during the study are deposited in the Gene Expression Omnibus – NCBI (accession number GSE311189 – send on November 24, 2025 and released on May 5, 2026. Link: https://www.ncbi.nlm.nih.gov/geo/query/acc.cgi?acc=GSE311189).

Declarations

Ethics approval and consent to participate
The study protocol was subjected and approved by Research Committee 1305 of the Mexican Social Security Institute (CONBIOETICA15201122), with registration number R-2024–1305-054**.**

Consent for publication
Not applicable.

Competing interests
The authors declare no competing interests.

Author details
[1]Programa de Doctorado en Ciencias en Biología Molecular en Medicina, Centro Universitario de Ciencias de la Salud (CUCS), Universidad de Guadalajara, Guadalajara, Jalisco 44340, Mexico
[2]División de Inmunología, Centro de Investigación Biomédica de Occidente (CIBO), Instituto Mexicano del Seguro Social (IMSS), Guadalajara, Jalisco 44340, Mexico
[3]Centro de Investigación y Asistencia en Tecnología y Diseño del Estado de Jalisco A.C. (CIATEJ), Guadalajara 44270, Mexico
[4]Programa de Doctorado en Ciencias Biomédicas, Centro Universitario de Ciencias de la Salud (CUCS), Universidad de Guadalajara, Guadalajara, Jalisco 44340, Mexico
[5]Instituto de Investigación en Ciencias Biomédicas, Centro Universitario de Ciencias de la Salud, Universidad de Guadalajara, Guadalajara 44340, Mexico
[6]Unidad de Investigación Epidemiológica y en Servicios de Salud, Instituto Mexicano del Seguro Social (IMSS), Guadalajara, Jalisco 44340, Mexico

Received: 14 April 2026 / Accepted: 9 July 2026
Published online: 28 July 2026

References

1. Li Z, Liu P, Yin A, Zhang B, Xu J, Chen Z, et al. Global landscape of cervical cancer incidence and mortality in 2022 and predictions to 2030: The urgent need to address inequalities in cervical cancer. Int J Cancer. 2025;157(2):288–97.
2. Singh D, Vignat J, Lorenzoni V, Eslahi M, Ginsburg O, Lauby-Secretan B, et al. Global estimates of incidence and mortality of cervical cancer in 2020: a baseline analysis of the WHO global cervical cancer elimination initiative. Lancet Glob Health. 2020;11(2):e197–206.
3. Huang J, Deng Y, Boakye D, Tin MS, Lok V, Zhang L, et al. Global distribution, risk factors, and recent trends for cervical cancer: A worldwide country-level analysis. Gynecol Oncol. 2022;164(1):85–92.
4. Pimple S, Mishra G. Cancer cervix: Epidemiology and disease burden. Cytojournal. 2022;19:21.
5. Ye J, Zheng L, He Y, Qi X. Human papillomavirus associated cervical lesion: pathogenesis and therapeutic interventions. MedComm (2020). 2020;4(5):e368.
6. Yu L, Majerciak V, Zheng ZM. HPV16 and HPV18 genome structure, expression, and post-transcriptional regulation. Int J Mol Sci. 2022. https://doi.org/10.3390/ijms23094943.
7. Hareza DA, Wilczynski JR, Paradowska E. Human papillomaviruses as infectious agents in gynecological cancers. Oncogenic properties of viral proteins. Int J Mol Sci. 2022;23(3):1818.
8. Wang X, Huang X, Zhang Y. Involvement of human papillomaviruses in cervical cancer. Front Microbiol. 2018;9:2896.
9. Okunade KS. Human papillomavirus and cervical cancer. J Obstet Gynaecol. 2020;40(5):602–8.
10. Munger K, Scheffner M, Huibregtse JM, Howley PM. Interactions of HPV E6 and E7 oncoproteins with tumour suppressor gene products. Cancer Surv. 1992;12:197–217.
11. DeFilippis RA, Goodwin EC, Wu L, DiMaio D. Endogenous human papillomavirus E6 and E7 proteins differentially regulate proliferation, senescence, and apoptosis in HeLa cervical carcinoma cells. J Virol. 2003;77(2):1551–63.
12. Yugawa T, Kiyono T. Molecular mechanisms of cervical carcinogenesis by high-risk human papillomaviruses: novel functions of E6 and E7 oncoproteins. Rev Med Virol. 2009;19(2):97–113.
13. Pal A, Kundu R. Human papillomavirus E6 and E7: the cervical cancer hallmarks and targets for therapy. Front Microbiol. 2019;10:3116.
14. Obanya DI, Wootton LM, Morgan EL. Advances in understanding the mechanisms of the human papillomavirus oncoproteins. Biochem Soc Trans. 2025;53(3):565–77.
15. George IA, Chauhan R, Dhawale RE, Iyer R, Limaye S, Sankaranarayanan R, et al. Insights into therapy resistance in cervical cancer. Adv Cancer Biol-Met. 2022;6:100074.
16. Burmeister CA, Khan SF, Schafer G, Mbatani N, Adams T, Moodley J, et al. Cervical cancer therapies: Current challenges and future perspectives. Tumour Virus Res. 2022;13:200238.
17. Das S, Babu A, Medha T, Ramanathan G, Mukherjee AG, Wanjari UR, et al. Molecular mechanisms augmenting resistance to current therapies in clinics among cervical cancer patients. Med Oncol. 2023;40(5):149.
18. Wong YMA, Ahn S, Bana A, Dua PK, Eggers R, Kuruvilla S, et al. Policy implications of WHO's Global traditional medicine strategy 2025–2034. Bull World Health Organ. 2025;103(11):715–21.
19. Asma ST, Acaroz U, Imre K, Morar A, Shah SRA, Hussain SZ, et al. Natural products/bioactive compounds as a source of anticancer drugs. Cancers (Basel). 2022. https://doi.org/10.3390/cancers14246203.
20. Ahmad M, Tahir M, Hong Z, Zia MA, Rafeeq H, Ahmad MS, et al. Plant and marine-derived natural products: sustainable pathways for future drug discovery and therapeutic development. Front Pharmacol. 2024;15:1497668.
21. Kangra K, Kakkar S, Mittal V, Kumar V, Aggarwal N, Chopra H, et al. Incredible use of plant-derived bioactives as anticancer agents. RSC Adv. 2025;15(3):1721–46.
22. Blowman K, Magalhaes M, Lemos MFL, Cabral C, Pires IM. Anticancer properties of essential oils and other natural products. Evid Based Complement Alternat Med. 2018;2018:3149362.
23. Amin A, Gali-Muhtasib H, Ocker M, Schneider-Stock R. Overview of major classes of plant-derived anticancer drugs. Int J Biomed Sci. 2009;5(1):1–11.
24. Altshuler O, Abu-Abied M, Chaimovitsh D, Shechter A, Frucht H, Dudai N, et al. Enantioselective effects of (+)- and (-)-citronellal on animal and plant microtubules. J Nat Prod. 2013;76(9):1598–604.
25. Sitarek P, Rijo P, Garcia C, Skala E, Kalemba D, Bialas AJ, et al. Antibacterial, anti-inflammatory, antioxidant, and antiproliferative properties of essential oils from hairy and normal roots of Leonurus sibiricus L. and their chemical composition. Oxid Med Cell Longev. 2017;2017:7384061.
26. Legault J, Dahl W, Debiton E, Pichette A, Madelmont JC. Antitumor activity of balsam fir oil: production of reactive oxygen species induced by alpha-humulene as possible mechanism of action. Planta Med. 2003;69(5):402–7.
27. Li Y, Li W, Ye Z, Ji C, Zhou Z. Antioxidant, anti-inflammatory, and anticancer activities of five citrus peel essential oils. Antioxidants (Basel). 2024. https://doi.org/10.3390/antiox13121562.
28. Zivkovic M, Stanisavljevic I, Gajovic N, Pavlovic S, Simovic Markovic B, Jovanovic IP, et al. Comprehensive phytochemical analysis and evaluation of antioxidant, antimicrobial, cytotoxic, and immunomodulatory activities of commercial cinnamon bark essential oil (Cinnamomum zeylanicum L.). Int J Mol Sci. 2025;26(13):6482.

29. Kallel I, Hadrich B, Gargouri B, Chaabane A, Lassoued S, Gdoura R, et al. Optimization of Cinnamon (Cinnamomum zeylanicum Blume) essential oil extraction: evaluation of antioxidant and antiproliferative effects. Evid Based Complement Alternat Med. 2019;2019:6498347.
30. Unlu M, Ergene E, Unlu GV, Zeytinoglu HS, Vural N. Composition, antimicrobial activity and in vitro cytotoxicity of essential oil from *Cinnamomum zeylanicum* Blume (Lauraceae). Food Chem Toxicol. 2010;48(11):3274–80.
31. Alizadeh Behbahani B, Falah F, Lavi Arab F, Vasiee M, Tabatabaee Yazdi F. Chemical composition and antioxidant, antimicrobial, and antiproliferative activities of *Cinnamomum zeylanicum* bark essential oil. Evid Based Complement Alternat Med. 2020;2020:5190603.
32. Kubatka P, Kello M, Kajo K, Samec M, Jasek K, Vybohova D, et al. Chemopreventive and therapeutic efficacy of *Cinnamomum zeylanicum* L. bark in experimental breast carcinoma: mechanistic in vivo and in vitro analyses. Molecules. 2020. https://doi.org/10.3390/molecules25061399.
33. Lin BH, Ma RX, Wu JT, Du SQ, Lv YY, Yu HN, et al. Cinnamaldehyde alleviates bone loss by targeting oxidative stress and mitochondrial damage via the Nrf2/HO-1 Pathway in BMSCs and Ovariectomized Mice. J Agric Food Chem. 2023.
34. Ke S, Zhu W, Lan Z, Zhang Y, Mo L, Zhu G, et al. Cinnamaldehyde regulates mitochondrial quality against hydrogen peroxide induced apoptosis in mouse lung mesenchymal stem cells via the PINK1/Parkin signaling pathway. PeerJ. 2022;10:e14045.
35. Lv C, Yuan X, Zeng HW, Liu RH, Zhang WD. Protective effect of cinnamaldehyde against glutamate-induced oxidative stress and apoptosis in PC12 cells. Eur J Pharmacol. 2017;815:487–94.
36. Ka H, Park HJ, Jung HJ, Choi JW, Cho KS, Ha J, et al. Cinnamaldehyde induces apoptosis by ROS-mediated mitochondrial permeability transition in human promyelocytic leukemia HL-60 cells. Cancer Lett. 2003;196(2):143–52.
37. Li W, Zhi W, Zhao J, Yao Q, Liu F, Niu X. Cinnamaldehyde protects VSMCs against ox-LDL-induced proliferation and migration through S arrest and inhibition of p38. JNK/MAPKs and NF-kappaB Vascul Pharmacol. 2018;108:57–66.
38. Wu CE, Zhuang YW, Zhou JY, Liu SL, Wang RP, Shu P. Cinnamaldehyde enhances apoptotic effect of oxaliplatin and reverses epithelial-mesenchymal transition and stemnness in hypoxic colorectal cancer cells. Exp Cell Res. 2019;383(1):111500.
39. Park J, Baek SH. Combination therapy with cinnamaldehyde and hyperthermia induces apoptosis of A549 non-small cell lung carcinoma cells via regulation of reactive oxygen species and mitogen-activated protein kinase family. Int J Mol Sci. 2020. https://doi.org/10.3390/ijms21176229.
40. Han L, Mei J, Ma J, Wang F, Gu Z, Li J, et al. Cinnamaldehyde induces endogenous apoptosis of the prostate cancer-associated fibroblasts via interfering the Glutathione-associated mitochondria function. Med Oncol. 2020;37(10):91.
41. Kim NY, Trinh NT, Ahn SG, Kim SA. Cinnamaldehyde protects against oxidative stress and inhibits the TNF-alpha-induced inflammatory response in human umbilical vein endothelial cells. Int J Mol Med. 2020;46(1):449–57.
42. Pina-Cruz R, Molina-Pineda A, Aguila-Estrada M, Villasenor-Garcia MM, Hernandez-Flores G, Jave-Suarez LF, et al. Effects of Arborvitae (Thuja plicata) essential oil on cervical cancer cells: insights into molecular mechanisms. Anticancer Agents Med Chem. 2024;24(20):1483–500.
43. Ulgen E, Ozisik O, Sezerman OU. pathfindR: An R package for comprehensive identification of enriched pathways in omics data through active subnetworks. Front Genet. 2019;10:858.
44. Xie GY, Ma J, Guan L, Liu XM, Wang A, Hu CH. Proliferation effects of cinnamon extract on human HeLa and HL-60 tumor cell lines. Eur Rev Med Pharmacol Sci. 2018;22(16):5347–54.
45. Koppikar SJ, Choudhari AS, Suryavanshi SA, Kumari S, Chattopadhyay S, Kaul-Ghanekar R. Aqueous cinnamon extract (ACE-c) from the bark of *Cinnamomum cassia* causes apoptosis in human cervical cancer cell line (SiHa) through loss of mitochondrial membrane potential. BMC Cancer. 2010;10:210.
46. Najar B, Shortrede JE, Pistelli L, Buhagiar J. Chemical composition and in vitro cytotoxic screening of sixteen commercial essential oils on five cancer cell lines. Chem Biodivers. 2020;17(1):e1900478.
47. Kumari S, Badana AK, G MM, G S, Malla R. Reactive oxygen species: a key constituent in cancer survival. Biomark Insights. 2018;13:1177271918755391.
48. Liou GY, Storz P. Reactive oxygen species in cancer. Free Radic Res. 2010;44(5):479–96.
49. Noh J, Kwon B, Han E, Park M, Yang W, Cho W, et al. Amplification of oxidative stress by a dual stimuli-responsive hybrid drug enhances cancer cell death. Nat Commun. 2015;6:6907.
50. Zou Z, Chang H, Li H, Wang S. Induction of reactive oxygen species: an emerging approach for cancer therapy. Apoptosis. 2017;22(11):1321–35.
51. Nile A, Shin J, Shin J, Park GS, Lee S, Lee JH, et al. Cinnamaldehyde-rich cinnamon extract induces cell death in colon cancer cell lines HCT 116 and HT-29. Int J Mol Sci. 2023. https://doi.org/10.3390/ijms24098191.
52. Li J, Teng Y, Liu S, Wang Z, Chen Y, Zhang Y, et al. Cinnamaldehyde affects the biological behavior of human colorectal cancer cells and induces apoptosis via inhibition of the PI3K/Akt signaling pathway. Oncol Rep. 2016;35(3):1501–10.
53. Ng LT, Wu SJ. Antiproliferative activity of cinnamomum cassia constituents and effects of Pifithrin-Alpha on their apoptotic signaling pathways in Hep G2 Cells. Evid Based Complement Alternat Med. 2011;2011:492148.
54. Liu Y, An T, Wan D, Yu B, Fan Y, Pei X. Targets and mechanism used by cinnamaldehyde, the main active ingredient in cinnamon, in the treatment of breast cancer. Front Pharmacol. 2020;11:582719.
55. Anju R, Sunitha MC, Nevin KG. Cinnamon extract enhances the mitochondrial reactive oxygen species production and arrests the proliferation of human colon cancer cell line, HCT-116. J Herbs Spices Med Plants. 2018;24:293–301.
56. Guan X, Su MC, Zhao RB, Ouyang HM, Dong XD, Hu P, et al. Cinnamon effectively inhibits the activity of leukemia stem cells. Genet Mol Res. 2016;15(3):2–17.
57. Abbasi A, Hajialyani M, Hosseinzadeh L, Jalilian F, Yaghmaei P, Jamshidi Navid S, et al. Evaluation of the cytotoxic and apoptogenic effects of cinnamaldehyde on U87MG cells alone and in combination with doxorubicin. Res Pharm Sci. 2020;15(1):26–35.
58. Aggarwal S, Bhadana K, Singh B, Rawat M, Mohammad T, Al-Keridis LA, et al. Cinnamomum zeylanicum extract and its bioactive component cinnamaldehyde show anti-tumor effects via inhibition of multiple cellular pathways. Front Pharmacol. 2022;13:918479.
59. Venkatraman M, Anto RJ, Nair A, Varghese M, Karunagaran D. Biological and chemical inhibitors of NF-kappaB sensitize SiHa cells to cisplatin-induced apoptosis. Mol Carcinog. 2005;44(1):51–9.
60. Filippova M, Filippov V, Williams VM, Zhang K, Kokoza A, Bashkirova S, et al. Cellular levels of oxidative stress affect the response of cervical cancer cells to chemotherapeutic agents. Biomed Res Int. 2014;2014:574659.
61. Leon CJ, Gomez SM, Morantes SJ, Cordero CP, Aristizabal FA. Sensitivity profile of a panel of cell lines designed for the evaluation of in vitro cytotoxicity. Biomedica. 2006;26(1):161–8.
62. Munoz-Espin D, Serrano M. Cellular senescence: from physiology to pathology. Nat Rev Mol Cell Biol. 2014;15(7):482–96.
63. Hernandez-Segura A, Nehme J, Demaria M. Hallmarks of cellular senescence. Trends Cell Biol. 2018;28(6):436–53.
64. Campisi J. Aging, cellular senescence, and cancer. Annu Rev Physiol. 2013;75:685–705.
65. Huang W, Hickson LJ, Eirin A, Kirkland JL, Lerman LO. Cellular senescence: the good, the bad and the unknown. Nat Rev Nephrol. 2022;18(10):611–27.
66. Kciuk M, Gielecinska A, Mujwar S, Kolat D, Kaluzinska-Kolat Z, Celik I, et al. doxorubicin-an agent with multiple mechanisms of anticancer Activity. Cells. 2023;12(4):659.
67. Mulati S, Shen F, Talihati Z, Zhang Y, Huang H, Zhang W. Targeting RPS16 with cinnamaldehyde to suppress cervical cancer: inhibition of the PI3K/AKT pathway and degradation of HPV E6 and E7 proteins. Biochem Pharmacol. 2025;242(Pt 1):117225.
68. Sehr P, Zumbach K, Pawlita M. A generic capture ELISA for recombinant proteins fused to glutathione S-transferase: validation for HPV serology. J Immunol Methods. 2001;253(1–2):153–62.
69. McLaughlin-Drubin ME, Munger K. The human papillomavirus E7 oncoprotein. Virology. 2009;384(2):335–44.
70. Meschede W, Zumbach K, Braspenning J, Scheffner M, Benitez-Bribiesca L, Luande J, et al. Antibodies against early proteins of human papillomaviruses as diagnostic markers for invasive cervical cancer. J Clin Microbiol. 1998;36(2):475–80.
71. Anderson M, Hrivnak W, Prak K, Stockert A. Potential effects of cinnamon on cancer prevention and progression. Front Nutr. 2025;12:1717834.
72. Luo D, Luo X, Xie J, Ye K, Wang X, Hu X, et al. Biological effects of cinnamaldehyde in animal cancer models: a systematic review and meta-analysis. Front Pharmacol. 2025;16:1557088.
73. Guo R, Wang R, Zhang W, Li Y, Wang Y, Wang H, et al. Multifaceted regulatory mechanisms of the EGR family in tumours and prospects for therapeutic applications (Review). Int J Mol Med. 2025;56(1):113.

74. Lipsick J. A history of cancer research: oncogenic transcription factors. Cold Spring Harb Perspect Biol. 2024. https://doi.org/10.1101/cshperspect.a035881.
75. Song B, Shen S, Fu S, Fu J. HSPA6 and its role in cancers and other diseases. Mol Biol Rep. 2022;49(11):10565–77.
76. Jain S, Rana M, Angmo N, Vimal N. The paradox of Heme Oxygenase 1: from cellular defense to a tug of war between cancer promotion and prevention. Adv Biol (Weinh). 2025;9(12):e00390.
77. Wu L, Xing P, Li J. DNAJA: emerging targets for anti-tumor therapy. Future Oncol. 2025;21(17):2251–9.
78. Liebermann DA, Tront JS, Sha X, Mukherjee K, Mohamed-Hadley A, Hoffman B. Gadd45 stress sensors in malignancy and leukemia. Crit Rev Oncog. 2011;16(1–2):129–40.
79. Diaz-Perez JA, Kerr DA. Gene of the month: DDIT3. J Clin Pathol. 2024;77(4):211–6.
80. Hicks D, Giresh K, Wrischnik LA, Weiser DC. The PPP1R15 Family of eIF2-alpha phosphatase targeting subunits (GADD34 and CReP). Int J Mol Sci. 2023;24(24):17321.
81. Uchi H, Yasumatsu M, Morino-Koga S, Mitoma C, Furue M. Inhibition of aryl hydrocarbon receptor signaling and induction of NRF2-mediated antioxidant activity by cinnamaldehyde in human keratinocytes. J Dermatol Sci. 2017;85(1):36–43.
82. O'Rourke SA, Shanley LC, Dunne A. The Nrf2-HO-1 system and inflammaging. Front Immunol. 2024;15:1457010.
83. Kadenbach B, Jarausch J, Hartmann R, Merle P. Separation of mammalian cytochrome c oxidase into 13 polypeptides by a sodium dodecyl sulfate-gel electrophoretic procedure. Anal Biochem. 1983;129(2):517–21.
84. Choi YH. Trans-cinnamaldehyde protects C2C12 myoblasts from DNA damage, mitochondrial dysfunction and apoptosis caused by oxidative stress through inhibiting ROS production. Genes Genomics. 2021;43(4):303–12.
85. Herrmann JM, Funes S. Biogenesis of cytochrome oxidase-sophisticated assembly lines in the mitochondrial inner membrane. Gene. 2005;354:43–52.
86. Gastwirt RF, McAndrew CW, Donoghue DJ. Speedy/RINGO regulation of CDKs in cell cycle, checkpoint activation and apoptosis. Cell Cycle. 2007;6(10):1188–93.
87. Zhao H, Xie Y, Yang Q, Cao Y, Tu H, Cao W, et al. Pharmacokinetic study of cinnamaldehyde in rats by GC-MS after oral and intravenous administration. J Pharm Biomed Anal. 2014;89:150–7.
88. Husain I, Gurley BJ, Kothapalli HB, Wang YH, Vedova LD, Chittiboyina AG, et al. Evaluation of bioaccessibility, metabolic clearance and interaction with xenobiotic receptors (PXR and AhR) of cinnamaldehyde. Food Chem (Oxf). 2025;10:100237.
89. Nir Y, Potasman I, Stermer E, Tabak M, Neeman I. Controlled trial of the effect of cinnamon extract on *Helicobacter pylori*. Helicobacter. 2000;5(2):94–7.
90. Altschuler JA, Casella SJ, MacKenzie TA, Curtis KM. The effect of cinnamon on A1C among adolescents with type 1 diabetes. Diabetes Care. 2007;30(4):813–6.
91. Crawford P. Effectiveness of cinnamon for lowering hemoglobin A1C in patients with type 2 diabetes: a randomized, controlled trial. J Am Board Fam Med. 2009;22(5):507–12.
92. Kort DH, Lobo RA. Preliminary evidence that cinnamon improves menstrual cyclicity in women with polycystic ovary syndrome: a randomized controlled trial. Am J Obstet Gynecol. 2014;211(5):487 e1-496.
93. Walanj S, Walanj A, Mohan V, Thakurdesai PA. Efficacy and safety of the topical use of intranasal cinnamon bark extract in seasonal allergic rhinitis patients: A double-blind placebo-controlled pilot study. J Herb Med. 2014;4:37–47.
94. Buckle J. Clinical aromatherapy: essential oils in healthcare. 3 ed. Elsevier; 2015.

Publisher's Note

Springer Nature remains neutral with regard to jurisdictional claims in published maps and institutional affiliations.